

High Resolution of Long Lead Time Ensemble Daily Rainfall Forecasts

A thesis submitted in part fulfilment of the degree of
Master of Machine Learning and Computer Vision

by
Weifan Jiang
U6683698

Supervisor: Dr. Warren Jin
Examiner: Dr. Zhenchang Xing



**Australian
National
University**

College of Engineering and Computer Science
The Australian National University

January 2022

This thesis does not contain content acceptable in any other university for the award of a degree or a diploma. It contains no previously publicated or written content to the best of the knowledge of the author, unless the appropriate citation is provided in the text.

Weifan Jiang
31 January 2022

Acknowledgements

First and foremost, I want to express my gratitude to my supervisor, Dr. Jin, for allowing me to discuss and address problems with him in a timely manner. He is a patient and conscientious supervisor. It is a privilege for me to meet him. Please allow me to convey my heartfelt appreciation one more. Three years of study life are coming to a close, three years of study life are being reviewed, and the sensation is fairly deep, with a bountiful harvest. There are many challenges in the thesis writing procedure, whether it is in the theoretical study stage or in the paper subject selection, data check four polls, opening, research, and writing every link, all of which get supervisor's supervision and assistance. Take advantage of this opportunity to express our heartfelt gratitude to you for allowing me to tutor at the same time. He is a laid-back enthusiast who pays close attention to detail. During the ICDM paper we completed and submitted together, Dr Jin is serious and responsible and always offers me deep and extensive direction, his to professional standards are always rigours with you, starting from the decision and fixed, until the final of the paper again and again modification, polishing.

Besides, I would like to thank Australia National University for allowing me to learn professional knowledge and how research knowledge and skills from them because of their mission, knowledge, and solutions.

I want to thank my parents for providing spiritual help in times of difficulty. Thanks to my friends for providing me with some inspiration based on their knowledge when I encountered a bottleneck.

Abstract

Downscaling has become a hot research content in super-resolution and analysis and computer vision because of its high application value in many real-life scenarios. When it applies to rainfall forecasts, This will have immeasurable value to people's lives and climate-sensitive industries, such as agriculture, mining and constructions. However, the existing algorithms aim to downscale probabilistic forecasts in terms of statistics, which are time-consuming and do not have a skilful improvement. Concerning the deep learning method on rainfall forecasts, recent work focus on making a precision mapping from low resolution to high resolution where the ensemble is not considered as a fact. However, for the physical model of probabilistic prediction, it is also impossible to carry out information statistics. To this end, we apply the deep learning method to implement a downscaling model for the model with ensemble forecasts. After many repeated experiments, I proposed the VDSRd model to downscaling rainfall forecasts with 11 ensemble number and leading 217 days and achieved skill on 8.1% on first seven days forecasts on average and -4.9% on 217 days leading by CRPS skill score(Continuous Ranked Probability skill score).

Contents

Acknowledgements	i
Abstract	ii
List of Figures	vi
List of Tables	vii
List of Tables	vii
Nomenclature	viii
1 Introduction	1
1.1 Precipitation Forecasts	1
1.2 Downscaling and super-resolution	1
1.3 Thesis Outline	2
2 Literature Review	4
2.1 Downscaling	4
2.1.1 Quantile-quantile Mapping	4
2.1.2 Neuron Networks Approach	5
2.1.2.1 DeepSD	6
2.1.2.2 AGSD	6
2.1.2.3 ResLap	6
2.1.3 VALUE	7
2.1.3.1 PFST-LSTM	8
2.2 Super Resolution	8
2.2.1 Interpolation Approach	9
2.2.1.1 Bilinear Interpolation	9
2.2.1.2 Bicubic Interpolation	9
2.2.2 Neuron Network Approach	10
2.2.2.1 SRCNN	11
2.2.2.2 FSRCNN	11
2.2.3 Summary	11
3 Methodology	13
3.1 Dataset	13
3.1.1 ACCESS	13
3.1.1.1 Ensemble Members	13
3.1.1.2 Data Structures	13
3.1.2 BARRA	14

3.1.2.1	Data Structures	15
3.2	Our model	15
3.3	Experiment	16
3.3.1	Criteria	17
3.3.1.1	MAE	17
3.3.1.2	RMSE	17
3.3.1.3	CRPS	17
3.3.1.4	Skill Score	18
3.3.2	Experiment Settings	18
3.3.3	Training Setting and Platform	18
3.4	Summary	19
4	Results and Analysis	20
4.1	Experimental Results	20
4.1.1	MAE, MSE and CRPS	20
4.1.2	Skill Score	20
4.2	Map View of Results	23
4.3	Summary	23
5	Conclusions and Future Development	28
5.1	Future Work	28
5.1.1	Expand Ensemble Members	28
5.1.2	Network Architecture	28
5.1.3	Riginal sub-model	29
5.1.4	Optimization process	29
A	Appendix A: The position of fifty observation stations	30
B	Appendix B:	32
	Bibliography	34

List of Figures

2.1	DeepSD's stacked SRCNN structure. Precipitation data and elevation sub-image pare are the inputs. One 5*5 kernel convolutional layer with maxpooling. It is followed by a fully connected layer and a 1*1 kernel convolutional layer, and lastly a 5*5 kernel output layer. (?)	6
2.2	The AGSD network is depicted in this diagram. AGSD reconstructs the HR rain intensity using the LR precipitation, the topography, and other meteorological factors as inputs. Color is preferable. (Yu et al., 2021)	7
2.3	Demostration of ConvLSTM structures. (Chuyao et al., 2020)	8
2.4	Demonstration of SRCNN model. (Dong et al., 2015)	11
2.5	Network structure of FSRCNN. (Dong et al., 2016)	11
3.1	Data structures of ACCESS	14
3.2	Overview of BARRA. BARRA-R contains forecasts across Australia, New Zealand, and Southeast Asia with a 12-by-12km and over Perth, Adelaide, Sydney, and Tasmania with 1.5-by-1.5km.	15
3.3	BARRA-R output data file structure.	15
3.4	Neural Network Structure.	16
3.5	Hardware Platform.	18
3.6	Software environment.	19
4.1	The image shows the Oceanic Nino index from 1990 to nowadays.	20
4.2	The figure shows the line diagram of Mae along with the leading time. The yellow one is $VDSRd_{pr,pr}$ model and the grey one is our $VDSRd_{pr}$ model. the blue line is the climatology 11 model. and the orange line shows the Bicubic interpolation model. From top to bottom is 1997, 2010, and 2012 years.	21
4.3	The figure shows the line diagram of RMSE along with the leading time. The yellow one is $VDSRd_{pr,pr}$ model and the grey one is our $VDSRd_{pr}$ model. the blue line is the climatology 11 model. and the orange line shows the Bicubic interpolation model. From top to bottom is 1997, 2010, and 2012 years.	22
4.4	The figure shows the line diagram of $CRPS_{SS}$ along with the leading time. Blue, yellow, orange and grey line is bicubic interpolation model, Calibration model, $VDSRd_{pr}$ and $VDSRd_{pr,zg}$ against climatology 11 respectively. From top to bottom is 1997, 2010, and 2012 years.	24
4.5	$CRPS_{SS}$ as a function of lead time for bicubic, calibration and $VDSRd_{pr}$, and $VDSRd_{pr,zg}$ of daily accumulated rainfall totals. The light grey shade indicates the 90% confidence interval of $CRPS_{SS}$ calculated from all the grid points in Australia and all the 48 initialization dates, the dark grey shade indicates the 50% confidence interval, and the red line indicates the median.	25

4.6	CRPS Skill Score for lead time 0 to 45 days in average in Australia. Sub-figure a is whole Australia and b is important 50 observation station point.	26
4.7	Demonstration of rainfall forecast.	27
A.1	The position of fifty observation stations.(Li and Jin, 2020)	31
B.1	The position of fifty observation stations.(Li and Jin, 2020)	33

List of Tables

4.1 Comparison between 5 models on 3 measurements. The best model are highlighted.	21
4.2 shows that average skill score on	23

Nomenclature

GCM	Global Climate Models
RCM	Regional Climate Model
SCF	Seasonal Climate Forecasts
CRPS	Continuous Ranked Probability Score
$CRPS_{SS}$	Continuous Ranked Probability Skill Score
MOS	Model Output Statistics
CNN	Convolutional Neuron Networks
ACCESS	Australian Community Climate and Earth-System Simulator Seasonal model
BARRA	The Bureau of Meteorology Atmospheric high-resolution Regional Reanalysis for Australia

Introduction

1.1 Precipitation Forecasts

The global climate has been changing significantly over the last 100 years, marked by warming, which has had serious consequences for the ecology and environment, including rising sea levels, melting and retreating glaciers, and worsening deserts. Climate change is having a negative influence on societal wellbeing as temperatures increase and extreme occurrences grow more intense. For example, daily precipitation forecasts will benefit the entire agricultural, which will help farmers optimize their farm planning and management, and insurers and traders will adopt their pricing plans. For Australia as a whole, the potential annual value added to an efficient precipitation forecast is approximately 1.6 billion dollars for agriculture (Xu et al., 2007). In order to avoid further deterioration of the environment and to reduce the damage caused by climate and meteorological disasters, the mechanisms and causes of change at the global level should be studied in-depth, and future measures should be taken. The trend of change should be predicted. Therefore, the GCM(GCM) has become an important and irreplaceable research tool in the study of global change. Weather forecasts were based on synoptic concepts until the early 1950s. With the advancement of computer technology and detection technology, in addition to the traditional weather map method and mathematical, statistical method, detection data from weather radar and satellite are being used in forecasting activities, and a numerical forecasting method is being developed. The numerical weather forecast, also known as or a physical model like the thesis given above, is the third phase, and it is extensively employed across the world. This approach allows for the prediction of atmospheric physical processes by finding the law of conservation of atmospheric mass, energy, and momentum, as well as for the major improvement in weather forecast quality and the quantification of objective weather predictions. To put it another way, it is based on a mathematical model of atmospheric motion that uses current weather conditions as input data to construct weather forecasting procedures, which are often completed using supercomputers or computing clusters scattered across a number of frames. Usually, GCM is a probabilistic model. The output data contains a variety of possible ensemble members, which increase the difficulty and uncertainty of downscaling.

1.2 Downscaling and super-resolution

Downscaling may transform GCM-provided large-scale climate data into RCM (Regional Climate Model) data, such as temperature and precipitation. RCM is a valuable addition to ground stations because it can provide a continuous long-term series of regional rainfall, has a high temporal resolution, and has a high utilisation value (Tang et al., 2019).

The dynamic downscaling approach is mainly utilised for climate forecasting; specifically, the RCM linked with the GCM is used to estimate future regional climate change scenarios. This strategy is

based on the physical law's starting value and has a distinct physical significance. The information notice has no effect on it. It may be used in a variety of settings and has the benefit of being adaptable to different resolutions. The disadvantage is that the computations are time-consuming and complex. Statistical downscaling may be thought of as a supplement to or a parallel form of dynamic scaling. The basic principle of this method is that predictive factors and predictive observations were established on the basis of data items, linear or nonlinear statistical relationships between them, the prediction model of elements was set, quantitative predictions of elements and independent observations were established using the method of statistical experience. This sort of link may be tested and then used to the model's output to predict variables. To compensate for some of the disadvantages of dynamic downscaling, statistical downscaling employs a huge quantity of real-time data, has excellent computing efficiency, and may create meteorological components at high resolution or on a station size. At the moment, the downscaling approach combining statistics and dynamics is a mix of the benefits of the two approaches above, and it is more practicable in practice. The employment of a neural network approach to "statistics" out regional model output is our way to find potential statistical relationship. The statistical downscaling approach, in particular, employs years of statistical data to develop a statistical link between big and small scales, which is then tested and used in future forecasting. This research investigates this possible statistical link using neural networks, and downscaling can be stated similarly:

$$Y = D(X|\theta) \quad (1.1)$$

, where $D(\cdot)$ is the downscaling function and X, Y is low resolution and high resolution precipitation forecasts, θ is the parameters. Similar to downscaling, processing low-resolution images using software and image super-resolution algorithms had become a significant research area in order to increase picture resolution. The process of image super-resolution involves reconstructing a high-resolution image from a low-resolution picture. After many years of research, image super-resolution technology was developed in the 1960s. The technology has continued to advance, and the quality of reconstruction is improving. It has been highly regarded by researchers because of its advantages of ease of use, simple hardware, and inexpensive cost. With the development of deep learning, super-resolution by deep learning was flourished. Therefore, many downscale methods for weather prediction based on Deep Learning super-resolution technology have emerged.

For example, (Reichstein et al., 2019) elaborated on the total number of methodologies on the application of deep learning to weather forecasting. (Shi et al., 2017), and (Chuyao et al., 2020) uses RNN (Recurrent Neuron Networks) to implements encoding-forecasting structures to study temporal features and re-generate weather nowcasting, rather than research on seasonal probabilistic forecasts. (Pan et al., 2019) applies CNN to get high resolution rainfall image, but not mention ensemble members as well.

In this research, we combined factors of ensemble climate forecasts, downscale and super-resolution and implement high resolution of long lead time(seasonal) ensemble rainfall forecasts.

1.3 Thesis Outline

There are 7 chapters in this paper. Chapter 2, give basic information on resentful technology and an examination of some documents relating to downscaling, deep learning and super resolution. Chapter 3, describes the data set we are using and its preprocessing, the neural network's structural architecture, evaluation criteria we have used, the parameter setting and the experimental hardware and

software environment the Chapter 4 The results reveal some depending on the assessment criteria we have employed and the experimental control group discussions and comparisons. Chapter 5 The entire thesis and prospective future work must contain the conclusions.

Literature Review

As this paper is mainly about rainfall forecasts, in Section 2.1 roughly discusses downscaling techniques. The second part of this section, Section 2.2, describes the background and basic ideas of super resolution.

2.1 Downscaling

Statistical downscaling approaches have been developed based on the empirical link between large-scale atmospheric variables (GCM) and information (RCM).

2.1.1 Quantile-quantile Mapping

Quantile-mapping (QM) Or cumulative distribution function matching (CDF), a simple post-processing method and is a classic statistics downscaling method, specifically to correct the CDF of the predicted value based on the CDF of the observed value. (LEI et al., 2020) and (Piani et al., 2010) using the method successfully found a mapping process from low resolution and high-resolution precipitation forecasts. In the process of implementing QM, each forecasted value is mapped to the corresponding quantile on the CDF of the observed value(Piani et al., 2010). By developing a transfer function between simulated and observed precipitation, this approach corrects the simulated precipitation. The following are the specific methods:

- 1 **Matching by the Cumulative Distribution Function (CDF)** First, when selecting a precipitation point or period for precipitation data, simulated and observed precipitation is sorted by model, is deemed to be an effective precipitation day of precipitation with daily rainfall over a specific amount and is divided into several periods concurrently. In minimal interval approaches, linear interpolation is used. The cumulative probability value of each grid point is calculated in simulated precipitation, and precipitation interpolation is seen with the precipitation sequence of the modelling phase. The calculation technique is the following:

$$PDF(X) = \int_{x_1}^{x_2} f(X)dX \quad (2.1)$$

$$cdf(X) = \int_0^{threshold} pdf(X)dX$$

, X is the amount of precipitation. $pdf()$ is the frequency distribution of precipitation in $[x_1, x_2]$. $CDF()$ is the cumulative probability distribution when precipitation is less than a certain precipitation threshold. The cumulative probability will be one, if threshold is largest value of the precipitation data.

- 2 **Construct Transfrom Function** In theory, linear or non-linear models are used to determine the functional link of large-scale climatic information with local variables. As a result, there are

two types of transfer function approaches: linear and non-linear transfer function approaches. Linear regression comprising multi-linear regression, linear regression gradual and the primary analysis of components are the most often used approach. Sailor and Li(Sailor and Li, 1999) used multiple linear regression to simulate the temperature in the United States. Murphy (Murphy, 2000) used the same method to recreate average monthly precipitation and temperatures across Europe.

Transform Function is The distinction between each research. In general, the best threshold of cumulative precipitation probability is obtained by parameter optimizer. as an example:

$$Transform(x) = \begin{cases} a_0 \cdot x & , \quad x < x_{j\text{th}} \\ \frac{a_0+a_1}{2} \cdot x & , \quad x_{j\text{th}} \leq x \leq x_{i\text{th}} \\ a_1 \cdot x & , \quad x > x_{i\text{th}} \end{cases} \quad (2.2)$$

$$CDF_{\text{obs}}[Transform(x)] = CDF_{\text{sim}}(x) \quad (2.3)$$

, where $x_{j\text{th}}, i\text{th}$ represents the precipitation value in the j-th and i-th quantiles, a_0 and a_1 Represent the correction coefficients. CDF_{obs} and CDF_{sim} represent the cumulative probability distribution of observed precipitation interpolation and simulated precipitation respectively.

3 Grid correction After modelling phase, transfer function is obtained and apply it to correct the calibration precipitation one by one grid, and finally get the result of the precipitation correction:

However, as an unconditional method, QM does not need to preserve the correlation between the predicted value and the observed data pair. Therefore, sometimes QM may think the original data is wrong, which leads to the result that is not as satisfactory as the conditional method. In addition, QM is suitable for the post-processing of GCM precipitation. However, they found that although QM can correct deviations, it does not guarantee reliability and continuity of predictions (continuity refers to at least the same performance as climatological predictions). The reason for this is that QM cannot reasonably consider the correlation between the original simulated value and the observed value. In the application process of statistical downscaling, there will be some uncertainties in the simulation results, mainly including model input uncertainty and the uncertainty of the downscaling model. The input of the statistical downscaling model is mostly the GCM output, including the current scenario value and the estimated value of the future scenario, which is the primary source of uncertainty in the downscaling simulation. The reason is that there are insufficient estimates of the concentration of future atmospheric greenhouse gases, large variations in the calculation of global average radiative forcing, insufficient climate system data that can be used for climate research and simulation, and insufficient climate model systems for predicting future climate changes. The vague understanding of the magnitude of natural climate change has led to the uncertainty of climate change prediction.

2.1.2 Neuron Networks Approach

Approaches based on neuron networks aims to find a non-linear mapping function end-to-end between low resolution and high resolution precipitation forecasts. Although neural network can also be regarded as a non-linear function, sometimes it is classified as a non-linear method with statistical downscaling. Because of the hotness of deep learning and in order to distinguish it from statistical downscaling, I will base it on deep learning methods The downscaling is distinguished separately.

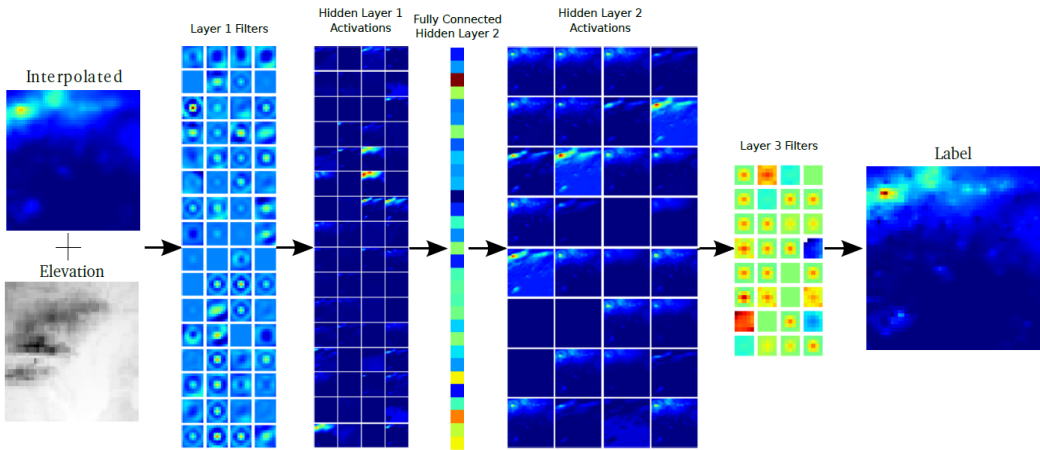


Figure 2.1: DeepSD’s stacked SRCNN structure. Precipitation data and elevation sub-image pare are the inputs. One 5×5 kernel convolutional layer with maxpooling. It is followed by a fully connected layer and a 1×1 kernel convolutional layer, and lastly a 5×5 kernel output layer. (?)

2.1.2.1 DeepSD

DeepSD is a CNN based precipitation downscaling approach aiming at acquiring high-resolution measurements. This is mostly represented in the data set’s creation. This dataset, like other super resolution datasets, employs an interpolation method to upsample meteorological parameters and achieve low resolution. After that, DeepSD suggested a generalised stacked super resolution convolutional neural network, which consisted of four SRCNNs layered on top of each other. Each upgraded SRCNN twice the quantity of precipitation data, resulting in an eight-fold increase in impact over low-resolution precipitation observations.

2.1.2.2 AGSD

Inspired by SR technology, a novel deep precipitation downscaling (DPD) approach termed auxiliary guided spatial distortion (AGSD) network is supposed by Yu et al. (Yu et al., 2021). An auxiliary guidance module (AGM) is presented, which uses numerous meteorological parameters as input to generate more accurate rain map characteristics (for example, temperature, relative humidity, and wind). A basic yet effective spatial distortion module (SDM) is also suggested at the same time. With the use of SDM, the DPD model can adjust the rain map using terrain correlation. A threat score was also included to improve the model’s performance under various rainfall intensities (including light rain, moderate rain, heavy rain, and storm).

AGM, SDM, HR reconstruction module (HR-rm), and pseudo TSLoss module are the four modules that makeup AGSD (PTSM). As input, SDM takes low-level meteorological and topography variables and outputs precipitation characteristics with topography a priori. AGM uses a variety of meteorological data as input, learning aids, and guidance to accomplish exact downscaling. These variables include temperature, relative humidity, wind, and so on. The outputs of SDM and AGM are combined in the final HR-input(Yu et al., 2021).

2.1.2.3 ResLap

ResLap is a technique for converting low spatial resolution climate data into high-resolution regional climate predictions. In the Laplacian Pyramid Super-Resolution Network, this approach primarily

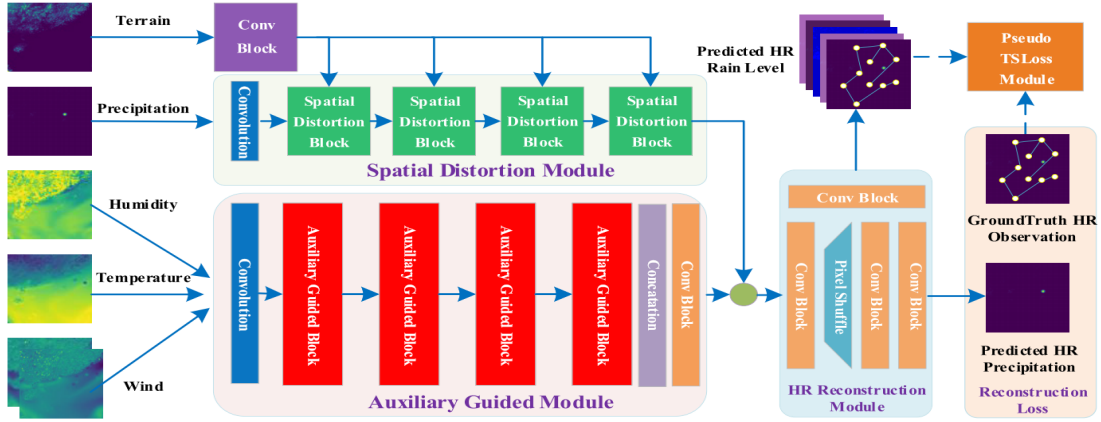


Figure 2.2: The AGSD network is depicted in this diagram. AGSD reconstructs the HR rain intensity using the LR precipitation, the topography, and other meteorological factors as inputs. Color is preferable. (Yu et al., 2021)

creates a new residual dense block (RDB) (LapSRN). Cheng et al. used RDB to fully extract hierarchical features from all convolutional layers, resulting in up-sampling picture reconstruction. This is supported by a significant number of experimental outcomes on the benchmark climatic data set. Climate data is also more difficult than conventional pictures due to its dynamic and chaotic character. We combined the original climate data given by the China Meteorological Administration and transformed it into trainable climate pictures to make model training easier. Finally, the resulting high-resolution climatic pictures are free of checkerboard artefacts. (Cheng et al., 2020). ResLap is a model that combines LapSRN and RDB and consists of two parts: feature extraction and image reconstruction. Among these, we employ RDB to exploit the hierarchical characteristics of each convolutional layer in feature extraction. We employ local residual learning to complete the fusion of all layers of up-sampled pictures in image reconstruction. ResLap's input and output are ILR and IsR, respectively.

2.1.3 VALUE

Bano-Medina et al. (Baño-Medina et al., 2020) think that due to their capacity to learn spatial characteristics from sizeable spatiotemporal data sets, deep learning techniques (particularly convolutional neural networks) have lately emerged as a potential statistical downscaling method. On the other hand, existing research is based on complicated models that are applied to specific case studies and verified using rudimentary frameworks, making it impossible to fully assess the (potential) additional value given by these technologies. The Value Cost Action (2012-2015) created a framework for verifying and comparing European downscaling solutions, emphasising diverse elements such as temporal and geographical structure and extreme scenarios.

Jorge et al. conducted a comprehensive assessment of the deep learning technology at the continental scale on the basis of the VALUE verification methodology. In particular, the low temperature, precipitation and standard VALUE benchmarking (linear and extended linear) techniques typically employed for this goal were applied to several sophisticated CNN models in Europe. The paper also looks at their extrapolation ability as the main feature of their prospective uses in climate change research, as well as assessing the appropriateness of different components and topological structures. The results demonstrate that the additional information goes. The results demonstrate that while the

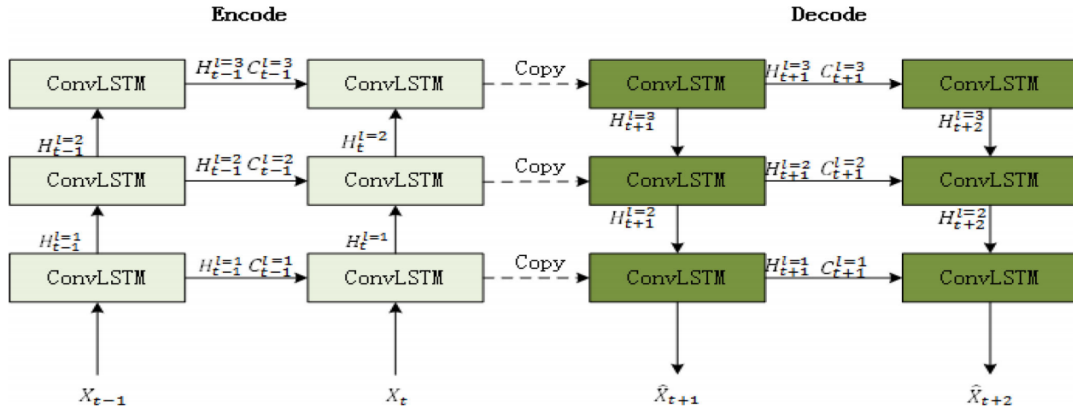


Figure 2.3: Demostration of ConvLSTM structures. (Chuyao et al., 2020)

added value of CNN is primarily restricted to the simulation of high temperatures, in most ways, these technologies under precipitation circumstances are superior to classical technologies. This generally good performance, plus it may be extended to more significant regions, such as continents, without concern for the spatial features, such as the coordinated regional experiment for climate reduction (CORDEX).

2.1.3.1 PFST-LSTM

Luo et al. proposed PFST-LSTM, which uses RNN to perform nowcast(Chuyao et al., 2020). This method not only maintains the fine-grained spatial appearance but also aligns the current observation result with the position when the previous hidden state is combined and has made a big breakthrough. Luo et al. propose a new convolutional RNN block that incorporates a spatial memory cell and a pseudo flow alignment module to alleviate the shortcomings of ConvLSTM.2.3

They build the PFST-LSTM sequence-to-sequence approach for radar echo map extrapolation on top of the block. The approach successfully combines spatial appearances and motion information, with the former being supplied in a zigzag direction and the latter being provided horizontally. Not only the space storage unit is embedded, but also the position alignment module is developed. These two unique designs can make up for the shortcomings of existing convolutional neural networks. Then stack the PFST-LSTM units into a sequence-to-sequence predictor. There are two elements to the predictor. One encoder collects spatial appearance traits and temporal dynamics from observed echogram sequences, while the other uses the retrieved data to forecast future echogram sequences. Finally, the down-sampling and up-sampling convolution kernels are put between the two PFST-LSTM layers in both the encoder and decoder.

On the MovingMNIST++ and CIKM AnalytiCup 2017 datasets, extensive empirical assessments are undertaken. Our results reveal that the suggested PFST-LSTM outperforms state-of-the-art approaches substantially.

2.2 Super Resolution

The conversion of low-resolution photographs to high-resolution pictures is known as super resolution. super resolution is recognised as the cause of a low-resolution picture:

$$LR = \mathcal{D}(HR; \theta) \quad (2.4)$$

, where D is mapping function, LR and HR is corresponding low resolution and high resolution image.

2.2.1 Interpolation Approach

In practise, we often meet image, transformation and so on in geometry space. In the source picture and the target picture the condition of these transactions is required to construct a mapping rule between

$$\text{left}(x\text{prime}, y\text{prime}) = T(x, Y)$$

that establishes for each pixel of the image destination a corresponding relation between the pixel coordinates.

Forward maping is a means to map the target image from the original image, although two problems may arise: Several pixels of the source frame are mapped to the same area on the target frame; there are no pixels to allocate in other portions of the target frame. The problem is, that several values can be converted into a single output value and pixels which are not connected to the target image can be assigned values. Examples of typical interpolation methods are nearest neighbour interpolation, bilinear interpolation and bicubic interpolation.

2.2.1.1 Bilinear Interpolation

Although the bilinear interpolation approach outperforms the closest interpolation approach, the difference is not significant. The closest interpolation technique simply uses one pixel's value, whereas bilinear interpolation, which use a weighted average technique and a linear equation:

$$y = y_1 \frac{(x - x_2)}{x_1 - x_2} + y_2 \frac{x - x_1}{x_2 - x_1}$$

, where (x, y) is target pixel that need to be assigned a value, $(x_1, y_1), (x_2, y_2)$ is the given value,to calculate the target pixel.

We name $f_h(i + u, j + v)$ as the target pixel. The four known pixel values next to the pixel are $f_l(i, j), f_l(i + 1, j), f_l(i, j + 1), f_l(i + 1, j + 1)$. The pixel weighted average of these four pixels is defined as:

$$f_h(i + u, j + v) = \omega_1 f_l(i, j) + \omega_2 f_l(i + 1, j) + \omega_3 f_l(i, j + 1) + \omega_4 f_l(i + 1, j + 1) \quad (2.5)$$

,where u and v are the horizontal distance between the target pixel and the left and the bottom margins of four surrounding areas, respectively. Therefore, $\omega_1, \omega_2, \omega_3, \omega_4$ define as: $\omega_1 = (1 - u)(1 - v)$, $\omega_2 = (u)(1 - v)$, $\omega_3 = (1 - u)v$, $\omega_4 = uv$.

2.2.1.2 Bicubic Interpolation

Bicubic Interpolation citepkeys1981cubic is the most difficult interpolation algorithm compared to the preceding two, but the image processing performance is greater, and it has become the most often used interpolation technique. Bicubic interpolation is the most used interpolation method in two-dimensional space in this discipline of mathematics. The value of the function f at the position (x, y) may be calculated using a weighted average of the nearest sixteen sample points.

For example, $f_h(i + u, j + v)$ is target pixel. To begin, determine the 16 pixels next to the target pixel and their values, and then use a weighted average to determine the values of these pixels.

The interpolation function is cubic polynomial, approximated from function $\frac{\sin(\pi*x)}{x}$ (Hou and Andrews, 1978), defined as $h(x)$:

$$h(x) = \begin{cases} (a+2)|x|^3 - (a+3)|x|^2 + 1 & , 0 < |x| \leq 1 \\ a|x|^3 - 5a|x|^2 + 8a|x| - 4a & , 1 < |x| < 2 \\ 0 & otherwise \end{cases} \quad (2.6)$$

where, a is commonly set to 0.5, and x is the difference between the target pixel position coordinates and four separate horizontal and vertical coordinates of 16 points (similar Equation ref2.6 and ref2.8). We can find out how much the 16 pixels around the target contribute to the target pixel by using the interpolation function. The target pixel may then be specified as follows:

$$f_h(i + u, j + v) = A^* B^* C \quad (2.7)$$

$$A = [h(u+1), h(u), h(u-1), h(u-2)] \quad (2.8)$$

$$B = \begin{bmatrix} f(i-1, j-1), f(i-1, j), f(i-1, j+1), f(i-1, j+2) \\ f(i, j-1), f(i, j), f(i, j+1), f(i, j+2) \\ f(i+1, j-1), f(i+1, j), f(i+1, j+1), f(i+1, j+2) \\ f(i+2, j-1), f(i+2, j), f(i+2, j+1), f(i+2, j+2) \end{bmatrix} \quad (2.9)$$

$$C = [h(v+1), h(v), h(v-1), h(v-2)]^T \quad (2.10)$$

Overall Equation 2.8 is equivalent to:

$$f(i + v, j + u) = \sum_{row=-1}^2 \sum_{col=-1}^2 f(i + row, j + col) h(row - v) h(col - u) \quad (2.11)$$

It does not describe a simple pixel surrounding the interpolation point, but rather considers a larger number of pixels. As a result, bicubic interpolation may be used to acquire more precise pixel values for the interpolation point. The bicubic interpolation approach, in comparison to the previous two interpolation methods, can recreate high-quality graphs.

2.2.2 Neuron Network Approach

Deep learning is advancing at a rapid pace, and neural networks are getting more sophisticated. This includes super resolution, which begins with the work of finding regressions and subsequently spreads out. supervised SR, unsupervised SR, and domain-specific SR are the three forms of super-resolution algorithms based on deep learning. As a result, we know that deep learning networks have a learning process. Deep Learning-based problems may be defined as (Wang et al., 2020) when combined with the Equation:

$$\hat{\theta} = \arg \min_{\theta} \mathcal{L}(SR, HR) + \lambda \Phi(\theta) \quad (2.12)$$

, L is loss function, computing error between high-resolution image and super-resolution image; λ is trade-off parameter and $\Phi(\theta)$ is regularisation term.

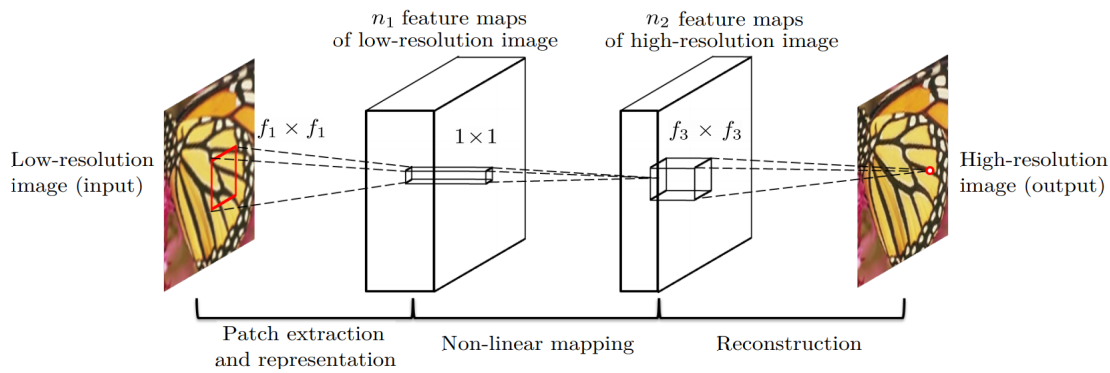


Figure 2.4: Demonstration of SRCNN model. (Dong et al., 2015)

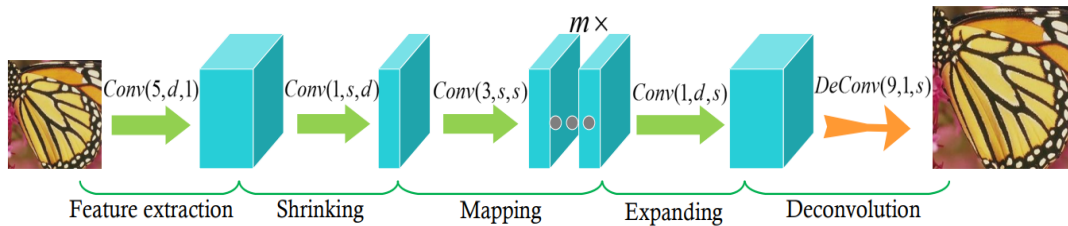


Figure 2.5: Network structure of FSRCNN. (Dong et al., 2016)

2.2.2.1 SRCNN

Deep learning is being applied for the first time in super-resolution reconstruction with the Super-Resolution Convolutional Neural Network (SRCNN). Three convolutional layers are used in SRCNN. The network structure is depicted in the diagram. 2.4. Structure of the three-layer convolution contains three steps: Patch extraction and feature representation, non-linear mapping and reconstruction.

2.2.2.2 FSRCNN

Fast Super-Resolution Convolutional Neural Network (FSRCNN) is a step forwards from the preceding (FSRCNN): To extend the size, transposed convolution is utilised. This allows the network to accept the original size of the image without having to expand the difference. To reduce computation complexity, use a 1*1 convolution kernel. In terms of training and forwards propagation, this makes the model quicker than SRCNN.

The model is made up of five pieces. The extraction of features is done using a 5-by-5 convolution kernel. Shrinking: The convolution layer with 1-by-1filter reduces the dimension of the feature map. Non-linear mapping is achieved using m convolutional layers with 3-by-3 kernels. Dimensional Expansion: For dimensional expansion, the 1-by-1 kernel convolution layer is used. To downsample the picture to the target size, use a transpose convolution. The network is organised as follows2.5:

2.2.3 Summary

We discovered in the preceding discussion that whether it is a downscale algorithm or a super-resolution algorithm, low-resolution images are converted into high-resolution images through a series of steps to make the high-resolution images similar to ground truth possible. In the preceding discussion, whether it is a downscale algorithm or a super-resolution algorithm, low-resolution pictures are converted into high-resolution pictures through a series of steps so that high-resolution pictures are as similar to

ground truth as possible. However, we can see that the current deep learning method mainly focuses on nowcasts and short period time of forecasts. None of them mentioned that application on probabilistic forecasts containing several ensemble members.

Methodology

Prior information and related studies can help us understand the potential of using artificial neural networks to downscale. In this chapter, I will start with the data to be inputted and detail the various aspects of the data set, then describe how to design and train my neural network after acquiring the necessary data and citing other scientists' contributions and my thinking in this part.

3.1 Dataset

3.1.1 ACCESS

In 2017, the Australian Meteorology Bureau announced the next generation access series GCM, which were later installed on supercomputers in the office in 2018. A worldwide combined model, the seasonal climate and earth system Simulator (ACCESS-S), is based on the UK's global combined seasonal prediction system glosea5-gc2. (Hudson et al., 2017).

3.1.1.1 Ensemble Members

The ACCESS-S contains 11 different ensemble members for seasonal forecasting (leading 217 days) due to disruptions and improved ensemble technology, including ten disturbed members and one unperturbed centre member. As the last chapter indicated before, both week and season are the ACCESS-S forecast time. Twenty-two ensemble members were formed from the 11-member ensemble for multi-week predictions (leading for six weeks). Every month, the 1st, 9th, 17th, and 25th hindcasts start from 1990 to 2012 because of the computational cost and limits of GloSea5-GC2. (Hudson et al., 2017).

3.1.1.2 Data Structures

As previously said, the model combines the atmosphere and the water, and its temporal range spans from every day to every season with 11 ensembles(Hawkins et al., 2013; Maraun, 2013).

MODEL NAME includes *raw model* with 60km Raw atmosphere and 25km Raw ocean surface model, atmospheric, terrestrial models, ocean and sea ice output. Both data sets are worldwide, with a grid of 60 km of atmosphere and a grid of 25 km of sea. It comprises a wide variety of three-dimensional variables, air surface and land surface temperature, humidity, sea surface temperature, etc. The *calibrated model* provides projections that comprise daily data over Australia on the 5-by-5km grid. The value of each grid was calibrated according to quantile methods of mapping.

PAR STREAM is the class parameter for: ocean parameters (*ocean*) and atmospheric parameters (*atoms*).

PAR is the parameter name: precipitation (*pr*), maximum temperature (*tasmax*), minimum temperature *tasmin*, geopotential height (*zg*), mean sea level pressure (*psl*), etc.

```

1 /g/data/ma05
2 .
3 |-- access-s1
4 |   '-- hc
5 |     |-- <MODEL NAME>
6 |     |   |-- <PAR STREAM>
7 |     |   |   |-- <PAR>
8 |     |   |   |   '-- <TIME SPAN>
9 |     |   |   |   '-- <ENSEMBLE MEMBER>
10 |
11 |   .
12 |   .
13 |   .
14 |   .
15 |   .

```

Figure 3.1: Data structures of ACCESS

TIME SPAN means the forecasts were generated *hourly, daily, weekly or monthly*.

ENSEMBLE MEMBER has 11 ensemble from e01 to e11.

Overall, although the resolution of the access output forecast is satisfactory in GCM, it falls short of the standards in regional climate prediction. As a result, the low-resolution input to the model will be these projected data. In the research, particularly, geopotential high at 850 hPa and precipitation in atoms of the ACCESS data are used for forward pass during training process.

3.1.2 BARRA

Bureau of Meteorology Atmospheric high-resolution Regional Reanalysis for Australia(BARRA) is Australia's regional climate prediction and numerical climate forecasts models based on an Australian area, using ACCESS-R, Australia's first atmospheric reanalysis model. ACCESS-R employs the UKMO system other than ACCESS-S. In addition, any uncertainty is not considered in this system. i.e. no ensemble member is present.

BARRA's weather on the surface and near the surface has been characterised by employing meteorological indicators such as temperature, wind velocity, surface pressures and rainfall. In addition, the 12-by-12 Km spatial resolution in Australia and New Zealand is implemented, and the 5-by-5 Km physical resolution in Australia's main cities is increased significantly by comparison with ACCESS-S. In regional review and high-resolution global simulations, the same approach applies to observations.

The reanalysis may be adequately represented by frequency distributions, extreme values and genuine space- and time-dependent variability. The Unified Model, a commonly used atmospheric grid point model, is utilised for BARRA. This model employs a sophisticated, non-fluid and compressible, kinetic atmospheric formula including mass conservation, time-integration methods, etc. (Acharya et al., 2019). BARRA data is our high-resolution image and considered as ground truth for our model.

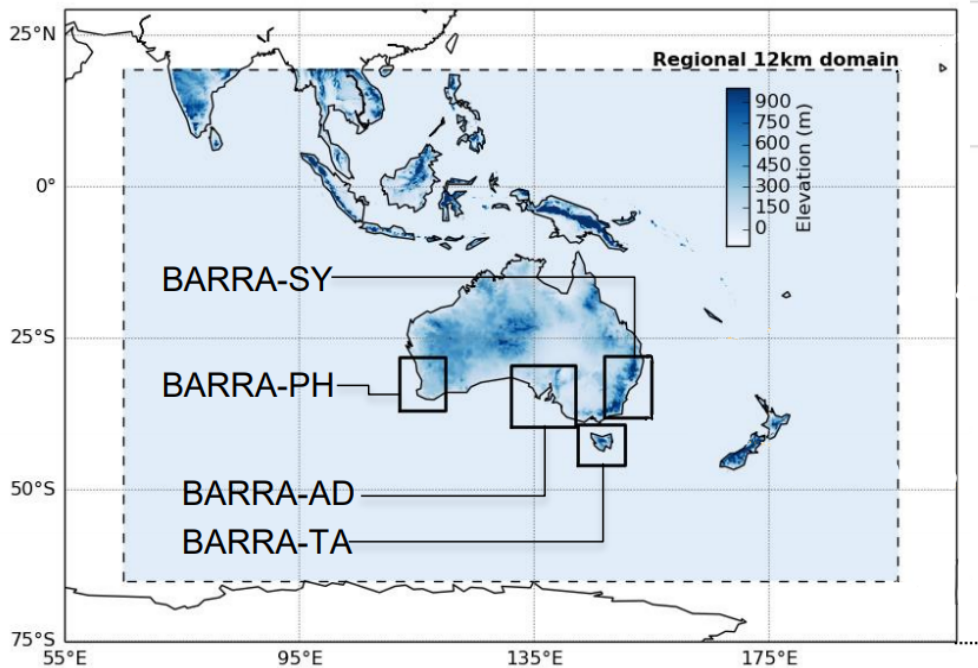


Figure 3.2: Overview of BARRA. BARRA-R contains forecasts across Australia, New Zealand, and Southeast Asia with a 12-by-12km and over Perth, Adelaide, Sydney, and Tasmania with 1.5-by-1.5km.

1 <PAR>-<PAR_STREAM>-spec-PT1H-<MODEL_DOMAIN>-v1-<Year><Month><Day>T<Timewindow>Z.sub.nc

Figure 3.3: BARRA-R output data file structure.

3.1.2.1 Data Structures

From above, BARRA is not a probabilistic forecasts model. And a data structures example shown as the figure 3.3, where

PAR is the parameter name: in particular, we use accumulated rainfall in a 6-hour time window (*accum_prcp*).

PAR STREAM is the parameter category: particularly, *spec* - Single level parameters available hourly sub-sampled from sub-hourly, surface and screen levels are used.

MODEL_DOMAIN the domain specific product name. It contains: *BARRA_R*, *BARRA_TA*, *BARRA_SY*, *BARRA_PH* or *BARRA_AD*.

Year,Month,day, denotes the valid year date of the forecast.

PAR is the indicator of each 4 accumulated rainfall image 6-hour time window, which contains 0000,0600,1200,1800

3.2 Our model

The network contains three parts: the input layer for feature extraction, the body network for generating high-level features and residual, and an output layer for regenerating the super-resolution image. To begin with, Bicubic interpolation is adopted to transfer size of LR (low resolution) image to the size of HR(High resolution). And given a daytime(t), ensemble number(en), and leading time(lt) then the

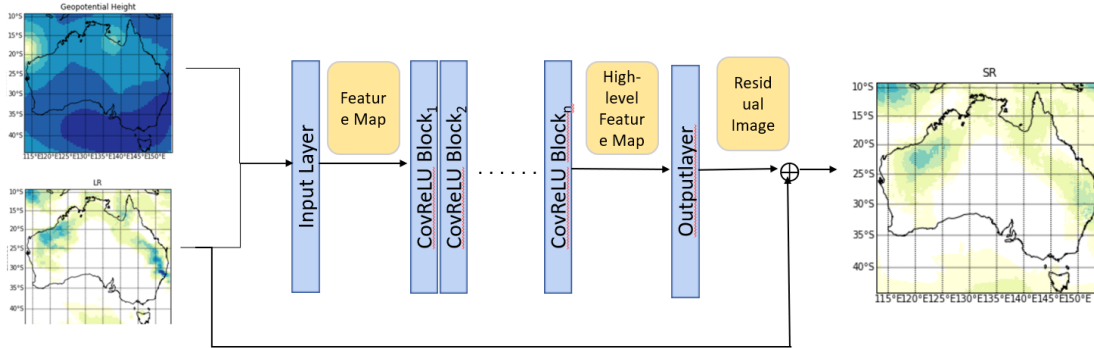


Figure 3.4: Neural Network Structure.

input layer can be expressed as:

$$FM_0^{en,t+lt} = \text{ReLU}(\text{Input}(BI(LR_{pr}^{en,t,lt}, LR_{zg}^{en,t,lt}))) \quad (3.1)$$

, where $\text{ReLU}()$ and $\text{Input}()$ is activation function and convolution layer with 3-by-3 filter Respectively. $BI()$ is bicubic interpolation, and LR_i is low resolution image coresponding to parameters i . In pricice, the pr and zg is abbreviation of Precipitation and Geopotential Height. In this process, zg and pr is considered as double-channel image. After input layer, the first Feature map (FM_0) is generated. for the following body network, it comes:

$$FM_i^{en,t+lt} = \text{ReLU}(\text{Conv}(M_i)), \quad i = 1, 2, 3, \dots, N$$

, where $\text{ReLU}()$ and $\text{Conv}()$ is activation function and convolution layer with 3-by-3 filter Respectively.

At last SR(super resolution) image is generated by:

$$SR^{en,t+lt} = FM_{-1}^{en,t+lt} + LR_{pr}^{en,t,lt}$$

, where FM_{-1} is feature map from output layer. The whole pipeline is shown at figure 3.4 This end-to-end model needs to learn and optimise several model parameters $\theta = \{W_{Input}, W_{Output}, W_1, W_2, \dots, W_n, B_{Input}, B_{Output}\}$. In practice, L1 loss is applied to optimize parameters. Given every batch of data, the training process can be expressed as:

$$\operatorname{argmin}_{\Theta} \sum_{batch=1}^B |SR_{batch}^{en,t+lt} - HR_{batch}^{t+lt}| = \operatorname{argmin}_{\Theta} \sum_{batch=1}^B |VDSRd(SR_{batch}^{en,t+lt}; \theta) - HR_{batch}^{t+lt}| \quad (3.2)$$

, where B indicate batch size and $| * |$ means taking the absolute value.

3.3 Experiment

In this section, MAE, RMSE, CRPS and CRPS are introduced to evaluate the model's performance. The first two evaluation criteria are for measuring the difference between the two images. CRPS is used as a standard evaluation method for downscaling and post-processing as well. And more detailed information concerning training setting and Platform will also be described in this section.

3.3.1 Criteria

3.3.1.1 MAE

The Mean Absolute Error is the average of the absolute values of the departures from the arithmetic mean in all individual observations. The average error can prevent mistakes from cancelling one another to precisely reflect the actual amount of the prediction mistake. Under this project context, the MAE can be defined as:

$$MAE_{i,j}^{lt} = \frac{1}{Init * Ens} \sum_{t=1}^{Init} \sum_{en=1}^{Ens} |SR_{i,j}^{en,t+lt} - HR_{i,j}^{t+lt}|$$

, where i,j for a grid index upon Australia region , we can calculate MAE among every initial date and ensembles.

3.3.1.2 RMSE

The root mean square error is the square root of the square deviation ratio between the forecast value and actual value of n:

$$RMSE_{i,j}^{lt} = \sqrt{\frac{1}{Init * Ens} \sum_{t=1}^{Init} \sum_{en=1}^{Ens} (F(LR^{en,t,lt}; \theta)_{i,j} - HR_{i,j}^{t+lt})^2}$$

, where i,j for a grid index upon Australia region , we can calculate RMSE among every initial date and ensembles.

The standard deviation in a measurement group is very sensitive to the big or little mistake and can thus represent measurement accuracy. This is why standard deviation in engineering are commonly utilised. The standard deviation is used to measure the degree of dispersion of a set of numbers, and the root means the square error is used to measure the deviation between the observed value and the actual value.

3.3.1.3 CRPS

Continuous ranking probability score (CRPS) is used to check probabilistic forecasts of continuous variables, as opposed to the MAE and RMSE. This indicator expresses the distance between the probabilistic forecast and the ground true value(Grimit et al., 2006; Unger, 1985). CRPS is the integral of the square of the difference in the real number domain between the cumulative distribution function and the Heaviside function. In the research context, given ensembles (Ens that equals 11), datetime (t) and leading time (lt):

$$CRPS_{i,j}^{lt} = \frac{1}{Ens * Init} \sum_{en=1}^{Ens} \sum_{t=1}^{Init} \int_{-\infty}^{\infty} [sCDF(SR_{i,j}^{en,t+lt}) - H(SR_{i,j}^{en,t,lt} < HR_{i,j}^{t+lt})]^2 d(SR^{t+lt}) \quad (3.3)$$

, where Heaviside function is:

$$H(*) = \begin{cases} 0 & , \text{Ture} \\ 1 & , \text{False} \end{cases} \quad (3.4)$$

, $sCDF$ is sorted Cumulative Probability Distribution along to ensemble members. The Euation means for every grid upon Australia region, we can calculate average CRPS among every initial date and ensembles.

	HPC(Gadi) in NCI	PC
CPU	24 * Intel(R) Xeon(R) Cascade Lake Platinum 8268	1 * Intel(R) Core(TM) CPU i5-9600K
CPU clock rate	2.9 GHz	3.70 GHZ
CPU logical cores	24	6
CPU cache	35.75 MB	9 MB
GPU	2 * Nvidia(R) Tesla Volta(TM) V100	1 * GeForce RTX 2070
GPU memory	32 GB	8 GB
CUDA(R) cores	5120	2304

Figure 3.5: Hardware Platform.

As shown above, it may be thought of as an extension of Mean Absolute Error (MAE) on continuous probability distributions. CRPS may be utilised as the probability model's loss function and evaluation function in practical applications, including probabilistic weather forecasting, error analysis, and anomaly identification. The result of assessing the probability model according to CRPS (pros and cons) is identical to the result of assessing the mathematical expectation of the probability model according to MAE as an evaluation function. CRPS is equivalent to the mean absolute error for a single value forecast.

3.3.1.4 Skill Score

Based on CRPS, we can define a Skill Score (SS) which represents how many improvement between two models.

$$CRPS_SS_{i,j}^{lt} = 1 - \frac{CRPS_{i,j}^{lt}}{CRPS_ref_{i,j}^{lt}} \quad (3.5)$$

where $CRPS_ref_{t+lt}$ is reference model, usually baseline model. Same to the MAE and RMSE, Calculation Skill score of MAE and RMSE are the same to CRPS_SS.

3.3.2 Experiment Settings

Total four control groups were set up to compare the performance of the model. The first is Climatology, which is often used to evaluate the quality of a downscaling method. Given a time windows w , this model uses the precipitation data of a total of w days before and after today in the history as ensemble members to calculate CRPS and be referred to the reference model in Equation 4.2

The second is the Bicubic interpolation model, which is widely used in super-resolution benchmarks.

The third is the Calibration model in ACCESS. The data is generated by Quantile mapping based on ACCESS-S.

The last model is the model without geopotential height(zg) parameters during the training.

3.3.3 Training Setting and Platform

The optimization strategy is SGD. The batch size is 32.the learning rate is set to 0.0001 and decays the learning rate of each parameter group by 0.99 every epoch. The training process was deployed

Package Name	ver.	Other
Torch	1.3.0-cuda	Model design, training ,testing
netCDF4	1.5.3	.nc file loading, saving
xarray	1.2.0	Processing of meteorological data after reading
basemap	1.2.1	Map drawing
matplotlib	3.1.3	Map and figure plotting
libtiff	0.4.2	Elevation data (DEM) reading

Figure 3.6: Software environment.

on NCI (National Computational Infrastructure). Its software environment and hardware is shown as Table 3.1 and 3.2:

3.4 Summary

Overall, the training pairs are generated from GCM, ACCESS-S, and RCM, BARRA-R, by re-location of the Australia regions. Our model is an end-to-end deep learning model. The input is pre-processed precipitation and geopotential height in ACCESS-S, and output is accumulated from 6-hour to daily precipitation of BARRA-R. The five models are used to compare their performance difference horizontally through 4 evaluation standards, MAE, RMSE, CPRS and skill score CRPS.

Results and Analysis

4.1 Experimental Results

In the section, the leave-one-year-out strategy was used for cross-validation on 1997, 2010 and 2012 to cover. The reason behind this is figure 4.1. 1997 is the strong El Niño phenomenon, 2010 contains strong La Niña, 2012 is the moderate year.

4.1.1 MAE, MSE and CRPS

Table 4.1 shows the comparisons with MAE, RMSE and MAE. The clear message is our model is better on Mae and RMSE. This means, on average, our precipitation forecasts themselves are closer to the ground truth value. Compare Bicubic and our model, and the conclusion is that deep learning indeed reduce the distance between inputs and output. The From Calibration model is generated using the downscaling method. Our model has exceeded the calibration model every year.

The figure 4.2 illustrates that result of MAE expanded along leading time. In terms of long-range of the leading time, the forecast with a larger leading trend to be unpredictable, our model's MAE goes up by around 0.25 from start to end. And other models see a 0.9 higher. Compare to the four models, and our model has a greater advantage. There are about 0.5 to 1.2 gaps between other models and my model from the gaps between each line. And the same phenomenon can be found in figure 4.3

4.1.2 Skill Score

Skill score tells how much improvement based on Climatology 11. From table 4.2, there is a non-positive improvement comparing to climatology 11, as climatology contains 242 ensemble members. Compared to the bicubic method, the deep learning model improves performance by approximately 10.7%, 5.3%, and 12.5% for 1997, 2010, 2012, respectively. Our model is still ahead of the existing

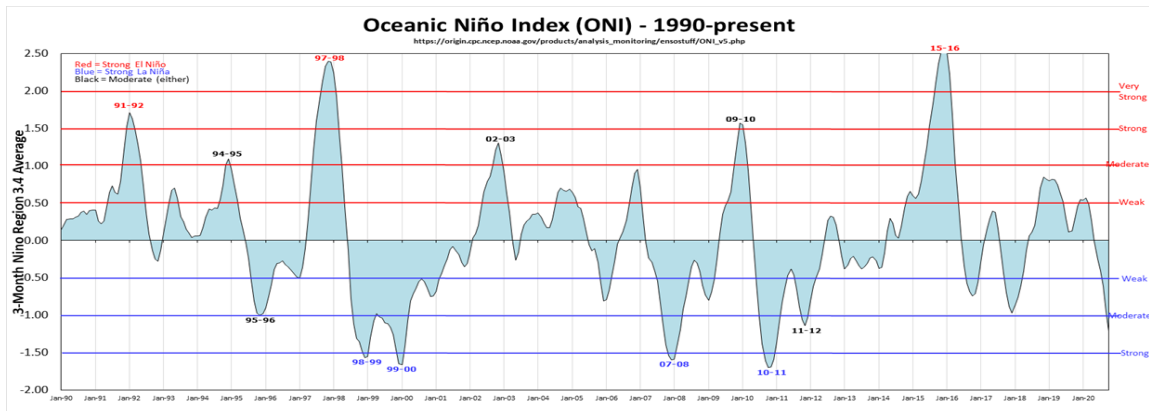
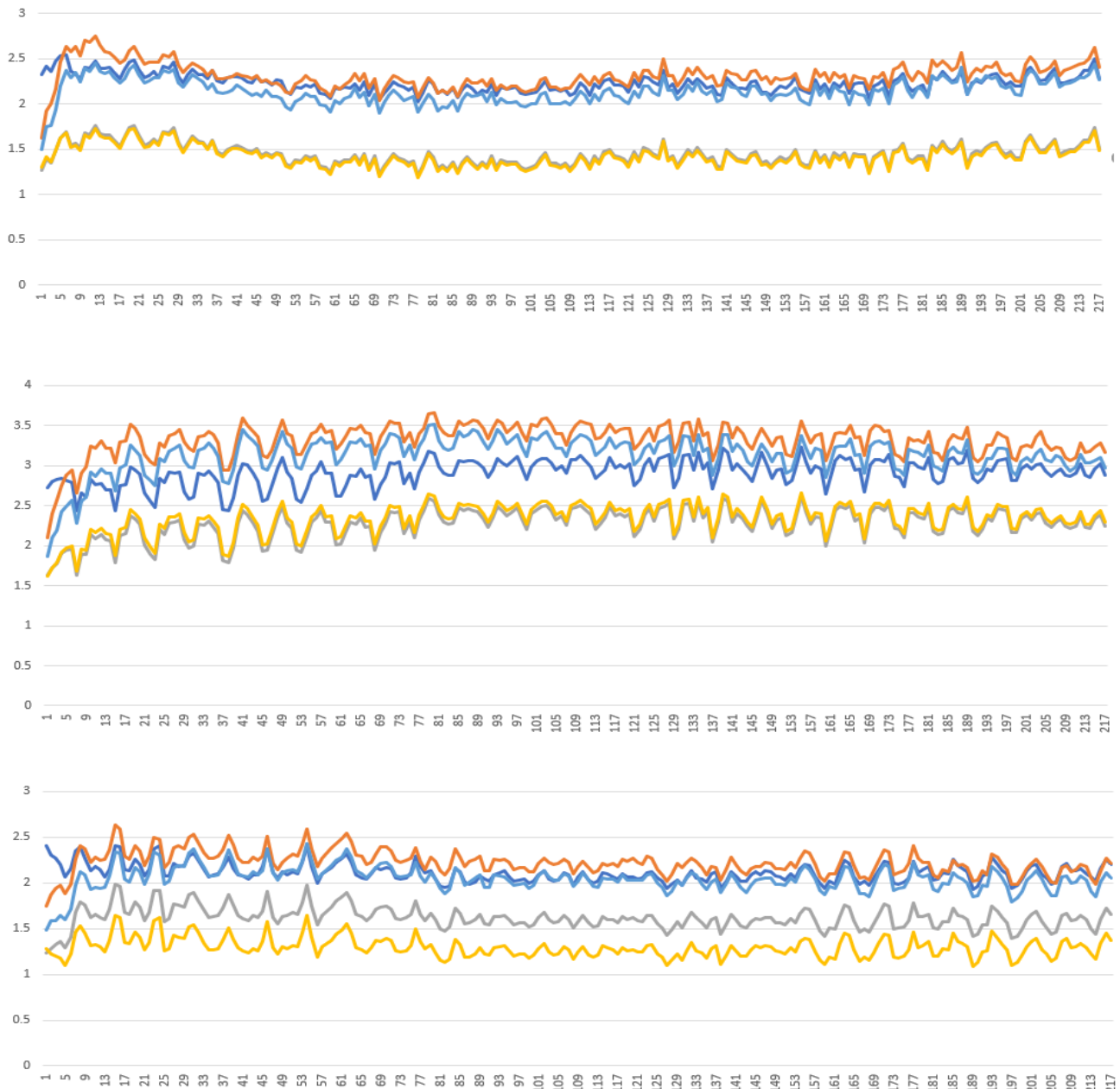


Figure 4.1: The image shows the Oceanic Niño index from 1990 to nowadays.

Model Name	1997			2010			2012		
	MAE	RMSE	CPRS	MAE	RMSE	CPRS	MAE	RMSE	CPRS
<i>Climatology</i> ₁₁	2.239	5.222	1.100	2.910	5.638	1.803	2.113	5.153	0.969
Bicubic	2.315	3.708	1.224	3.319	5.014	1.912	2.223	3.676	1.102
Calibration	2.143	3.367	1.208	3.134	4.582	1.922	2.047	3.315	1.088
<i>VDSRd_{pr}</i>	1.451	1.718	1.181	2.276	2.590	1.926	1.619	2.284	1.028
<i>VDSRd_{pr,zg}</i>	1.425	1.649	1.193	2.335	2.729	1.902	1.297	1.563	1.032

Table 4.1: Comparison between 5 models on 3 measurements. The best model are highlighted.

Figure 4.2: The figure shows the line diagram of Mae along with the leading time. The yellow one is *VDSRd_{pr,pr}* model and the grey one is our *VDSRd_{pr}* model. the blue line is the climatology 11 model. and the orange line shows the Bicubic interpolation model. From top to bottom is 1997, 2010, and 2012 years.

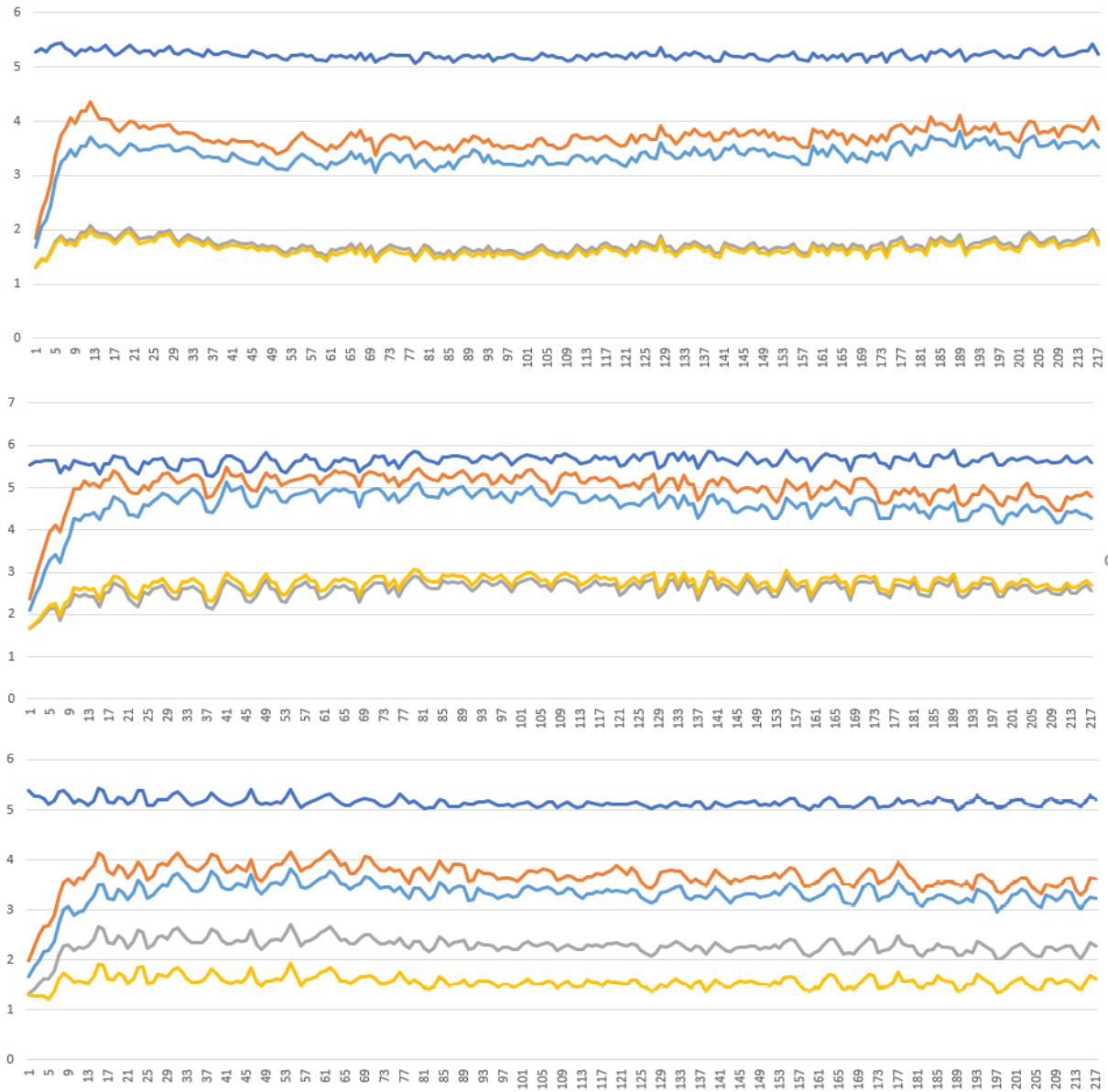


Figure 4.3: The figure shows the line diagram of RMSE along with the leading time. The yellow one is $VDSRd_{pr,pr}$ model and the grey one is our $VDSRd_{pr}$ model. the blue line is the climatology 11 model. and the orange line shows the Bicubic interpolation model. From top to bottom is 1997, 2010, and 2012 years.

Model Name	1997	2010	2012
Bicubic	-0.164	-0.104	-0.209
Calibration	-0.1375	-0.102	-0.168
VDSRd _{pr}	-0.057	-0.060	-0.0842
VDSRd _{pr,zg}	-0.067	-0.051	-0.0495

Table 4.2: shows that average skill score on

quantile mapping calibration model by approximately 8.0%, 4.2% and 11.9% for 1997, 2010 and 2012, respectively. By adding a geopotential height channel, there will be a negative increase in the El Niño year and a small amount of contribution in 2010 and 2012.

The figure 4.4 illustrates performance of different model on different leading time. In general, our model is in a leading position in all leadig time segments. From the day before yesterday, our model has a steady improvement of about 5 Between and 15%. In the following six months, all models have declined by varies.

probability sample's confidence interval is the interval estimate of a population parameter in the sample. The confidence interval reveals how much the real value of this parameter has a chance of falling around the measurement result, and it offers the confidence degree of the measured value of the measured parameter. In figure 4.5, Our curve is relatively stable compared to other models, and the width of each year is relatively narrow, which means that there is a small variance. The bicubic model has the highest 0.307 and lowest -0.631 on day 0, which is equivalent to 0.938 intervals, and Calibration is better than that of Bicubic coming 0.543 interval. Our model has 0.730 and 0.391 interval. In the value of 95%, Our model has a positive improvement throughout the whole process, while other models have not dropped below the x-axis for about the first seven days. Quantile number 75%, $VDSRd_{pr,zg}$ sometimes reaches a positive skill, which is also a good sign.

4.2 Map View of Results

the place marked as red is the place without improvement. So our model has a larger area of blue points. Our model has a 0.1 skill score for most areas on Australian land, with somewhat higher CRPS skill ratings in Western Australia. In addition, the same phenomenon can be seen on 50 important climate observation station.

Figure 4.7 illustrates rainfall forecast of low resolution, high resolution and our model for seven days. Notice that, as the effect of the ensemble, there is no perfect pixel-level match between the input and output. But we can still see that the super-resolution image has a displacement and value adjustment from low resolution to high resolution.

4.3 Summary

According to the aforementioned findings, our approach outperforms the Bicubic interpolation model statistically and performs similarly to the calibration model. From a regional standpoint, our model performs better on Australia's west coast than on its east coast. Our approach offers a significant increase in terms of time efficiency, confirming its usefulness. However, because our model is based on the super-resolution approach, the outcomes are very reliant on the input data. Furthermore, the data set's ambiguity makes it more difficult to forecast properly with our model.

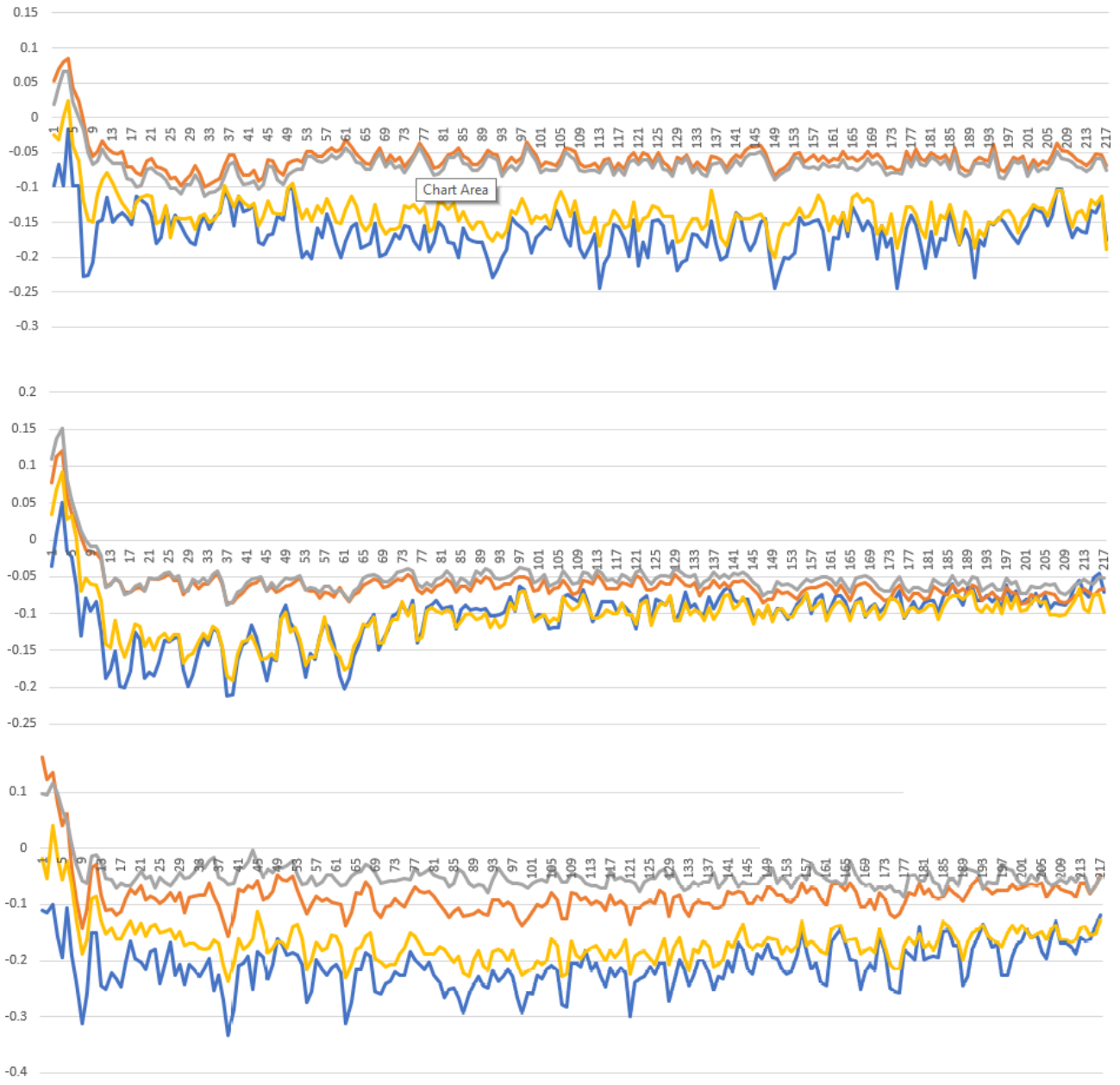


Figure 4.4: The figure shows the line diagram of $CRPS_{SS}$ along with the leading time. Blue, yellow, orange and grey line is bicubic interpolation model, Calibration model, $VDSRd_{pr}$ and $VDSRd_{pr,zg}$ against climatology 11 respectively. From top to bottom is 1997, 2010, and 2012 years.

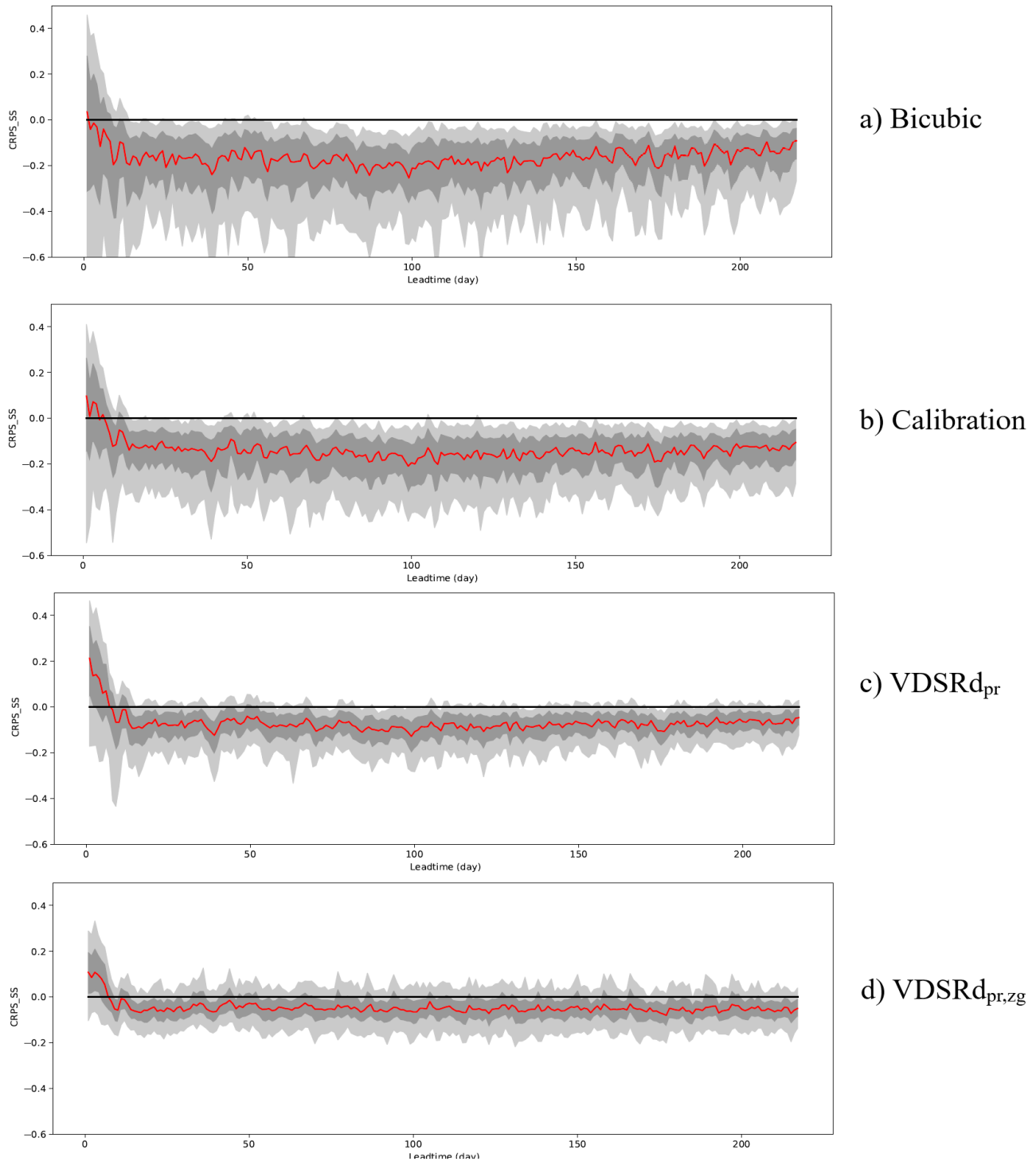


Figure 4.5: $CRPS_{SS}$ as a function of lead time for bicubic, calibration and $VDSRd_{pr}$, and $VDSRd_{pr,zg}$ of daily accumulated rainfall totals. The light grey shade indicates the 90% confidence interval of $CRPS_{SS}$ calculated from all the grid points in Australia and all the 48 initialization dates, the dark grey shade indicates the 50% confidence interval, and the red line indicates the median.

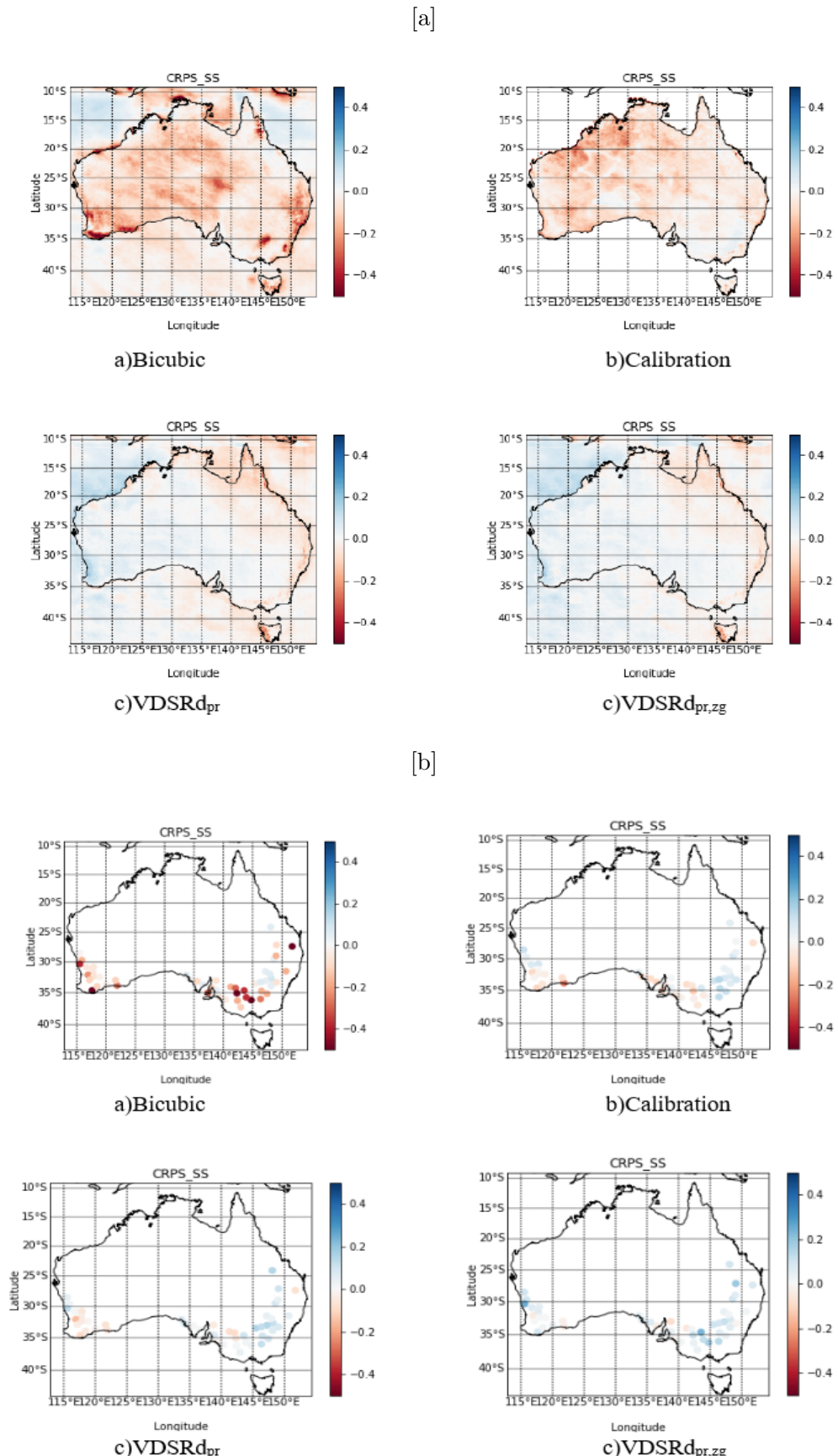


Figure 4.6: CRPS Skill Score for lead time 0 to 45 days in average in Australia. Sub-figure a is whole Australia and b is important 50 observation station point.

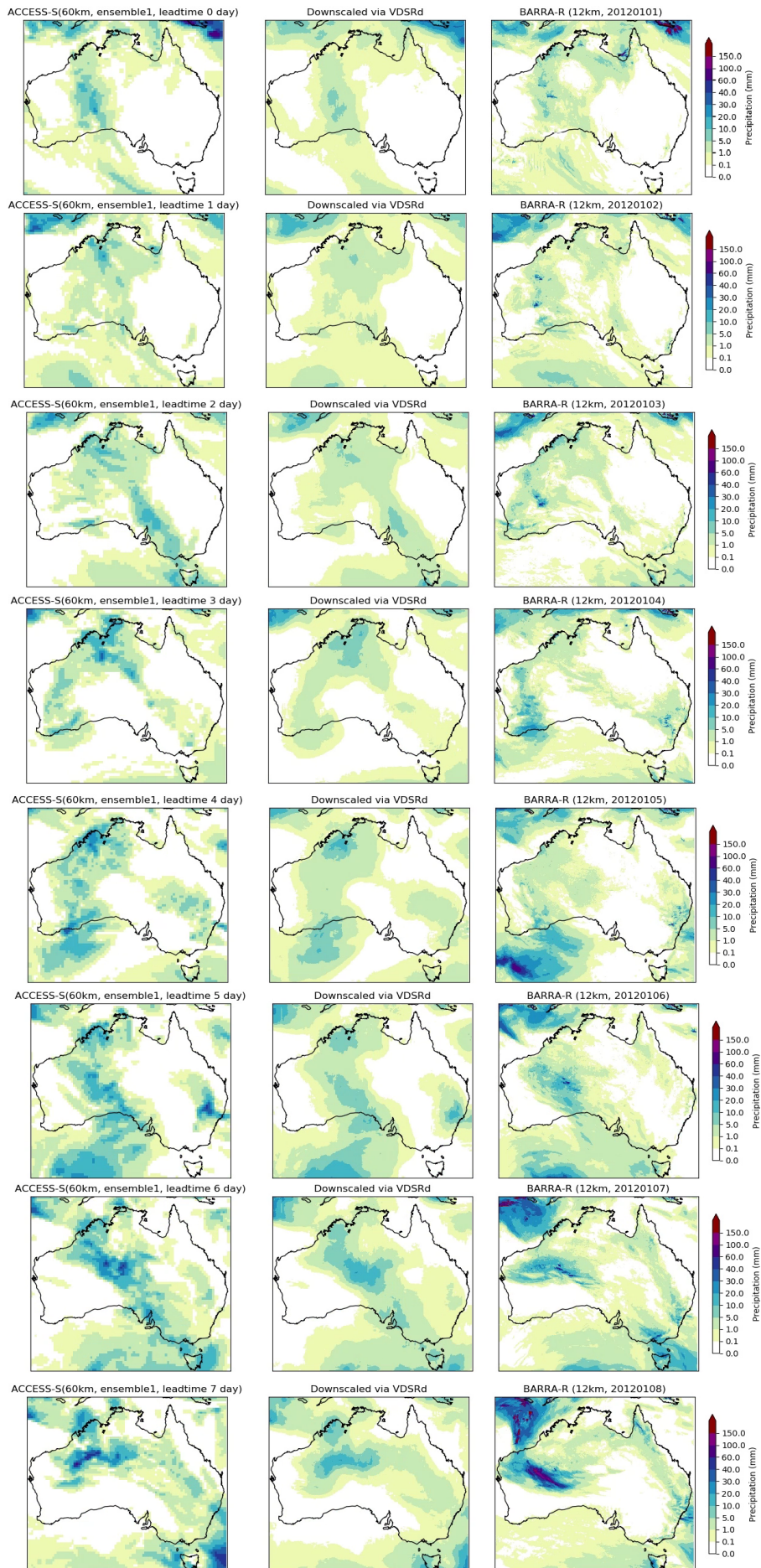


Figure 4.7: Demonstration of rainfall forecast.

Conclusions and Future Development

We discovered certain parallels between downscale and super-resolution through the chapter introduction and literature study, which formally confirms the rationale and practicality of our research. We used several representative single-image super-resolution forecasting methods and selected VDSRd as a suitable deep learning model, based on CRPS, by choosing comprehensive and general validation data sets for CRPS to improve the downscaling technology of Australia's long lead time ensemble daily rainfall forecast. In addition, climatic variables were added to the VDSRd, as well as extremely deep statistical downscaling.

The results described in the preceding chapter further demonstrate the applicability of the proposed approach, particularly the time efficiency increase. Furthermore, the comparison with the interpolation model demonstrates the availability of deep learning, implying that neural network learning contributes to bias correction. When compared to the Calibration model, the time cost is much reduced while the forecast accuracy and ensemble forecast skill are substantially improved.

5.1 Future Work

5.1.1 Expand Ensemble Members

We notice that in Table 4.1, climatology 11 used past data as ensemble members. They contain 242 ensembles. Comparing to the 11 ensembles we use, this is not a relatively fair comparison. Therefore, discovering and designing a method to extend the probabilistic prediction to the same number of ensembles will also help improve the performance of the model.

5.1.2 Network Architecture

Although our model is relatively good, the low-resolution ensemble forecasts map to the high-resolution rainfall forecasts. But we can see that the statistical laws and time-series information between the ensemble are not used well. In many nowcast-based methods, a large number of algorithms such as RNN and LSTM are used to obtain timing characteristics. In our long leading time ensemble forecasts, although there are many initial day and ensemble, the timing characteristics of the overall model performance There is huge potential for improvement.

The neural network is shown to be adaptable in this article. As a result, the next-generation neural network might be built on the Transposed convolution theory, which compresses the feature map in order to increase computation speed or model depth. Furthermore, a deeper network with theoretical underpinnings in the field of super-resolution models, such as and RNAN(Zhang et al., 2018, 2019), can be used. Deeper networks can capture more information, and their learning and generalisation abilities have both increased significantly(LeCun et al., 2015).

5.1.3 Riginal sub-model

The findings show that our model has a discernible variation in prediction performance between Australia's east and west coastlines. Various climatic trends in different places may be to blame. As a result, we may create a deep learning model for each region in order to characterise precipitation forecast in a given area. Due to the limits of GCM, there are 11 computations based on distinct physical models, producing 11 ensemble members, and 11 models can be constructed according to different ensemble series, as indicated in the data section.

5.1.4 Optimization process

During training, we find that even added a shortcut link from the input layer and output layer, the decay of gradient in backpropagation still cannot be prevented very effectively. At the same time, when the learning rate is too large, especially when the loss function is L2 loss function training, the gradient explosion phenomenon is particularly serious. This greatly affects the effect of the trained model. Therefore, you can try to use Adjustable Gradient Clipping to avoid the model over the best point. The starting point is very simple: if the gradient becomes very large, then we adjust it to keep it small. Gradient clipping ensures the maximum norm of the gradient vector (specified as c in this article). Even when the loss function of the model is irregular, this technique helps gradient descent maintain reasonable behaviour. The picture below shows the cliff of the loss function. Without clipping, the parameters will change drastically along the gradient descent direction, causing them to leave the minimum range; and after clipping, the parameter changes will be limited to a reasonable range, avoiding the above situation. Therefore, for larger gradients, set the cropping threshold so that the cropped gradient will not be greater than this threshold in order to solve the problem that the explosion causes the model to be difficult to train.

From the evaluation criteria, the loss function does not punish the probability distribution well, so the simple l1 loss cannot explain the distribution information well. Therefore discover a suitable loss function to punish the ensembles whose distribution gap is too large, and pull in the distance between the prediction and the ground truth in the probability distribution. Besides, in this part, I have done some experiments and got some preliminary results, and I am going to add it to the comparison with VDSRd in all aspects.

Appendix A: The position of fifty observation stations

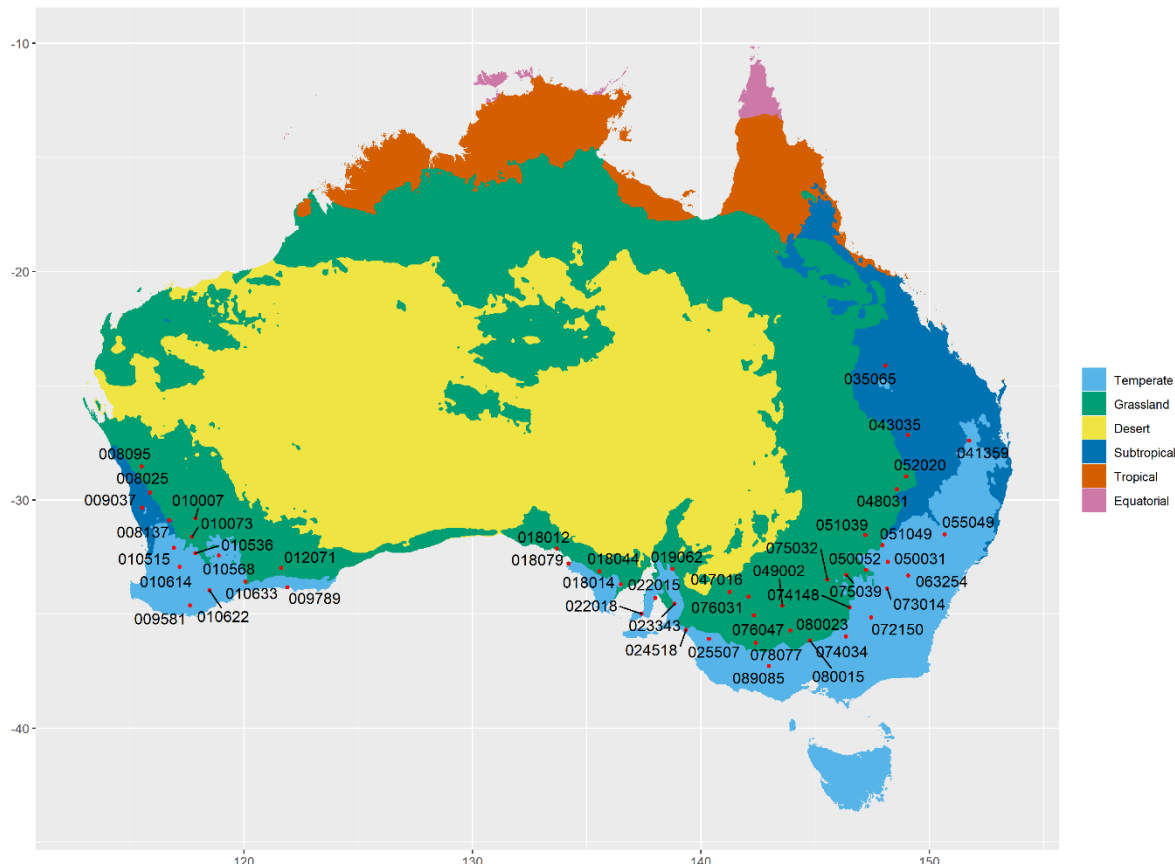


Figure A.1: The position of fifty observation stations.(Li and Jin, 2020)

Appendix B:

StationCode	StationName	State	Soil	Cultivar	Lat	Lon	climate.region	climate.charac	annualRainfall	rainday-prop
1 000825	CARNAMAH	WA	Northern Tenosol	Endure	-29.6886	115.8872	Grassland	hot (summer drought)	337.793577933379	0.22250251850613
2 0008055	MULLEWA	WA	Northern Tenosol	Derrimut	-28.5367	115.5142	Grassland	hot (summer drought)	332.831686713964	0.18712058832228
3 0008137	WONGAN HILLS	WA	Northern Kandosol	Endure	-30.8917	116.7186	Subtropical	distinctly dry summer	388.0574336538853	0.24163790024997
4 0009337	BAUDINGGARRA RESEARCH STN	WA	Northern Tenosol	Correll	-30.3381	115.5394	Subtropical	distinctly dry summer	515.7400904655421	0.290203547196762
5 0009581	MOUNT BARKER	WA	Southern Sodosol	Bolac	-34.625	117.6361	Temperate	distinctly dry (and warm) summer	651.682061659326	0.472800857704828
6 009789	ESPERANCE	WA	Southern Sodosol	Endure	-33.83	121.8925	Temperate	distinctly dry (and warm) summer	609.242828234734	0.3659008820378526
7 010007	BENCUBBIN	WA	Northern Kandosol	Wyalkatchem	-30.8081	117.8603	Grassland	hot (summer drought)	305.942209260802	0.2421140343566
8 010073	KELLERBERRIN	WA	Northern Chromosol	Wyalkatchem	-31.6183	117.7217	Grassland	warm (summer drought)	310.047907479705	0.207951434353053
9 010515	BEVERLEY	WA	Northern Chromosol	Endure	-32.1083	116.9247	Temperate	distinctly dry (and hot) summer	410.5978545494584	0.25116057612189
10 010536	CORRIGIN	WA	Southern Sodosol	Wyalkatchem	-32.3292	117.7333	Temperate	distinctly dry (and hot) summer	352.5300610601125963	0.2530061060588025
11 010568	HYDEN	WA	Southern Kandosol	Derrimut	-32.4419	118.8983	Temperate	distinctly dry (and hot) summer	365.53202702059248	0.2453271937150339
12 010614	NARROGIN	WA	Southern Chromosol	Endure	-32.9342	117.1797	Temperate	distinctly dry (and hot) summer	448.7014998214203	0.285532175812403
13 010622	ONGERUP	WA	Southern Sodosol	Correll	-33.9644	118.4889	Temperate	distinctly dry (and warm) summer	395.304428044248	0.3540054755388626
14 010633	RAVENSTHORPE	WA	Southern Sodosol	Endure	-33.5803	120.0458	Grassland	warm (persistently dry)	446.676407570527	0.344601833115105
15 012071	SALMON GUMS RES.STN.	WA	Southern Sodosol	Correll	-32.9869	121.6239	Grassland	warm (persistently dry)	379.176824187597	0.287108677538388
16 018012	CEDUNA AMO	SA	Northern Calcarosol	Wyalkatchem	-32.1297	133.6976	Grassland	warm (summer drought)	270.993274610165	0.2421140343566
17 018014	CLEVE	SA	Southern Calcarosol	Endure	-33.7011	136.4937	Temperate	distinctly dry (and hot) summer	400.552850851089	0.36124235210094
18 018044	KYANCUTTA	SA	Southern Calcarosol	Derrimut	-33.1337	135.5521	Grassland	warm (summer drought)	299.024770860612	0.255564813712653
19 018079	STREAKY BAY	SA	Southern Calcarosol	Endure	-32.7963	134.2116	Temperate	distinctly dry (and hot) summer	370.817581240329	0.302225925485061
20 019062	YONGALA	SA	Southern Calcariosol	Wyalkatchem	-33.0276	138.7576	Grassland	warm (persistently dry)	362.610760623735	0.269610760623735
21 022015	PRICE	SA	Southern Calcariosol	Bolac	-34.2971	138.0014	Grassland	warm (summer drought)	338.7775264849423	0.2704439941762528
22 022018	WAROOKA	SA	Southern Calcariosol	Bolac	-34.9906	137.3995	Temperate	distinctly dry (and warm) summer	459.1066539869765	0.357576478990506
23 023343	ROSEDALE (TURRETTFIELD RESEARCH CENTRE)	SA	Southern Calcariosol	Bolac	-34.5519	138.8342	Temperate	distinctly dry (and hot) summer	480.7433633885252	0.32019997619331
24 024518	MENINGIE	SA	Southern Calcariosol	Endure	-35.6902	139.3375	Temperate	distinctly dry (and warm) summer	457.820616593263	0.39281037791767
25 025507	KEITH	SA	Southern Tenosol	Endure	-36.098	140.3556	Temperate	distinctly dry (and warm) summer	436.214319723842	0.336626592972372
26 035065	SPRINGTURE COMET ST	QLD	Northern Vertosol	Wyalkatchem	-24.123	148.0856	Subtropical	moderately dry winter	712.338709677419	0.190096417093203
27 041359	OAKLEY AERO	QLD	Northern Vertosol	Wyalkatchem	-27.4034	151.7413	Temperate	no dry season (hot summer)	578.582061659326	0.216402809189382
28 043035	SURAT	QLD	Northern Dermosol	Wyalkatchem	-27.1591	149.0702	Grassland	hot (persistently dry)	569.39739316748	0.192506119509582
29 047016	LAKE VICTORIA STORAGE	NSW	Southern Calcariosol	Wyalkatchem	-34.0438	141.2676	Grassland	warm (persistently dry)	258.367515771932	0.190096417093203
30 048031	COLLARENEBRI (ALBERT ST)	NSW	Southern Calcariosol	Wyalkatchem	-34.5407	148.5818	Grassland	hot (persistently dry)	564.566063563861	0.1798539540530889
31 049001	BALRANAL (RSI)	NSW	Southern Calcariosol	Wyalkatchem	-34.6398	143.561	Grassland	warm (persistently dry)	339.987441971194	0.218069274766968
32 050031	PEAK HILL POST OFFICE	NSW	Southern Chromosol	Wyalkatchem	-32.7235	148.1902	Temperate	no dry season (hot summer)	578.317105106335	0.22056897230092
33 050032	CONDOBOLIN AG RESEARCH STN	NSW	Southern Chromosol	Wyalkatchem	-33.0664	147.2283	Grassland	warm (persistently dry)	448.166646827759	0.23401975952434
34 051039	NYNGAN AIRPORT	NSW	Northern Chromosol	Wyalkatchem	-31.5495	147.1961	Grassland	hot (persistently dry)	486.30895131532	0.18057374121283
35 051049	TRANGIE RESEARCH STATION AWS	NSW	Northern Vertosol	Wyalkatchem	-31.9861	147.9489	Temperate	no dry season (hot summer)	499.169325080348	0.207951434353053
36 052020	MUNGINDI POST OFFICE	NSW	Northern Vertosol	Wyalkatchem	-28.9756	148.8999	Grassland	hot (persistently dry)	512.75267230092	0.17735983811451
37 050549	QUIRINDI POST OFFICE	NSW	Northern Vertosol	Wyalkatchem	-31.5086	150.6792	Temperate	no dry season (hot summer)	693.9952098178788	0.2491913700499107
38 063254	ORANGE AGRICULTURAL INSTITUTE	NSW	Southern Chromosol	Wyalkatchem	-33.3211	149.0828	Temperate	no dry season (warm summer)	936.70784668492	0.42268777564849
39 072150	WAGGA WAGGA AMO	NSW	Southern Chromosol	Correll	-35.1583	147.4575	Temperate	no dry season (hot summer)	569.5884001904535	0.277347393476967
40 073014	GREENFELL (MANGANESE RD)	NSW	Southern Chromosol	Wyalkatchem	-33.8034	148.1523	Temperate	no dry season (hot summer)	621.50790329473	0.281037971670039
41 074034	COROWA AIRPORT	NSW	Southern Chromosol	Endure	-35.9887	146.3574	Temperate	no dry season (hot summer)	556.919354833871	0.18497797812046
42 074148	NARRANDERA AIRPORT AWS	NSW	Southern Chromosol	Wyalkatchem	-34.705	146.5154	Grassland	warm (persistently dry)	430.409772646114	0.2291393388168075
43 075032	HILSTON AIRPORT	NSW	Southern Chromosol	Wyalkatchem	-33.4915	145.5248	Grassland	warm (persistently dry)	398.128496607547	0.17605047182121
44 075039	LAKE CARGELLIIGO AIRPORT	NSW	Southern Calcariosol	Wyalkatchem	-33.2832	146.3706	Grassland	warm (persistently dry)	420.825318414474	0.1886608015712415
45 076031	MILDURA AIRPORT	VIC	Southern Calcariosol	Wyalkatchem	-34.2358	142.0867	Grassland	warm (persistently dry)	286.690751101059	0.18497797812046
46 076047	OUYER (POST OFFICE)	VIC	Southern Vertosol	Bolac	-36.2614	142.405	Grassland	warm (persistently dry)	323.247232472325	0.224854184025711
47 078077	WARRACKNAEAL MUSEUM	VIC	Southern Sodosol	Derrimut	-36.1647	144.7642	Grassland	warm (persistently dry)	380.523687656231	0.27591953388882
48 080015	ECHUCA AERODROME	VIC	Southern Sodosol	Bolac	-35.7236	143.9197	Grassland	warm (persistently dry)	404.73247234723	0.30912986549203
49 080023	KERANG	VIC	Southern Vertosol	Endure	-37.2769	142.9786	Temperate	no dry season (warm summer)	378.846625401738	0.2392573128199
50 089085	AIRARAI PRISON	VIC	Southern Sodosol						555.38123651946	0.409117962147363

Figure B.1: The position of fifty observation stations.(Li and Jin, 2020)

Bibliography

- ACHARYA, S. C.; NATHAN, R.; WANG, Q. J.; SU, C.-H.; AND EIZENBERG, N., 2019. An evaluation of daily precipitation from a regional atmospheric reanalysis over australia. (2019).
- BAÑO-MEDINA, J.; MANZANAS, R.; AND GUTIÉRREZ, J. M., 2020. Configuration and intercomparison of deep learning neural models for statistical downscaling. *Geoscientific Model Development*, 13, 4 (2020), 2109–2124.
- CHENG, J.; KUANG, Q.; SHEN, C.; LIU, J.; TAN, X.; AND LIU, W., 2020. Reslap: Generating high-resolution climate prediction through image super-resolution. *IEEE Access*, 8 (2020), 39623–39634.
- CHUYAO, L.; LI, X.; AND YE, Y., 2020. Pfst-lstm: a spatiotemporal lstm model with pseudo-flow prediction for precipitation nowcasting. *IEEE Journal of Selected Topics in Applied Earth Observations and Remote Sensing*, (2020).
- DONG, C.; LOY, C. C.; HE, K.; AND TANG, X., 2015. Image super-resolution using deep convolutional networks. *IEEE transactions on pattern analysis and machine intelligence*, 38, 2 (2015), 295–307.
- DONG, C.; LOY, C. C.; AND TANG, X., 2016. Accelerating the super-resolution convolutional neural network. In *European conference on computer vision*, 391–407. Springer.
- GRIMIT, E. P.; GNEITING, T.; BERROCAL, V. J.; AND JOHNSON, N. A., 2006. The continuous ranked probability score for circular variables and its application to mesoscale forecast ensemble verification. *Quarterly Journal of the Royal Meteorological Society: A journal of the atmospheric sciences, applied meteorology and physical oceanography*, 132, 621C (2006), 2925–2942.
- HAWKINS, E.; OSBORNE, T. M.; HO, C. K.; AND CHALLINOR, A. J., 2013. Calibration and bias correction of climate projections for crop modelling: an idealised case study over europe. *Agricultural and forest meteorology*, 170 (2013), 19–31.
- HOU, H. AND ANDREWS, H., 1978. Cubic splines for image interpolation and digital filtering. *IEEE Transactions on acoustics, speech, and signal processing*, 26, 6 (1978), 508–517.
- HUDSON, D.; ALVES, O.; HENDON, H. H.; LIM, E.-P.; LIU, G.; LUO, J.-J.; MACLACHLAN, C.; MARSHALL, A. G.; SHI, L.; WANG, G.; ET AL., 2017. Access-s1: the new bureau of meteorology multi-week to seasonal prediction system. *Journal of Southern Hemisphere Earth Systems Science*, 67, 3 (2017), 132–159.
- LECUN, Y.; BENGIO, Y.; AND HINTON, G., 2015. Deep learning. *nature*, 521, 7553 (2015), 436–444.
- LEI, H.; MA, J.; LI, H.; WANG, J.; SHAO, D.; AND ZHAO, H., 2020. Bias correction of climate model precipitation in the upper heihe river basin based on quantile mapping method. *Plateau Meteorology*, 39, 2 (2020), 266–279.

- LI, M. AND JIN, H., 2020. Development of a postprocessing system of daily rainfall forecasts for seasonal crop prediction in australia. (2020).
- MARAUN, D., 2013. Bias correction, quantile mapping, and downscaling: Revisiting the inflation issue. *Journal of Climate*, 26, 6 (2013), 2137–2143.
- MURPHY, J., 2000. Predictions of climate change over europe using statistical and dynamical downscaling techniques. *International Journal of Climatology: A Journal of the Royal Meteorological Society*, 20, 5 (2000), 489–501.
- PAN, B.; HSU, K.; AGHAKOUCHAK, A.; AND SOROOSHIAN, S., 2019. Improving precipitation estimation using convolutional neural network. *Water Resources Research*, 55, 3 (2019), 2301–2321.
- PIANI, C.; HAERTER, J.; AND COPPOLA, E., 2010. Statistical bias correction for daily precipitation in regional climate models over europe. *Theoretical and Applied Climatology*, 99, 1 (2010), 187–192.
- REICHSTEIN, M.; CAMPS-VALLS, G.; STEVENS, B.; JUNG, M.; DENZLER, J.; CARVALHAIS, N.; ET AL., 2019. Deep learning and process understanding for data-driven earth system science. *Nature*, 566, 7743 (2019), 195–204.
- SAILOR, D. J. AND LI, X., 1999. A semiempirical downscaling approach for predicting regional temperature impacts associated with climatic change. *Journal of Climate*, 12, 1 (1999), 103–114.
- SHI, X.; GAO, Z.; LAUSEN, L.; WANG, H.; YEUNG, D.-Y.; WONG, W.-K.; AND WOO, W.-C., 2017. Deep learning for precipitation nowcasting: A benchmark and a new model. *arXiv preprint arXiv:1706.03458*, (2017).
- TANG, X.; ZHANG, J.; WANG, G.; YANG, Q.; YANG, Y.; GUAN, T.; LIU, C.; JIN, J.; LIU, Y.; AND BAO, Z., 2019. Evaluating suitability of multiple precipitation products for the lancang river basin. *Chinese geographical science*, 29, 1 (2019), 37–57.
- UNGER, D., 1985. A method to estimate the continuous ranked probability score. preprints. In *Ninth Conf. on Probability and Statistics in Atmospheric Sciences*, 206–213.
- WANG, Z.; CHEN, J.; AND HOI, S. C., 2020. Deep learning for image super-resolution: A survey. *IEEE Transactions on Pattern Analysis and Machine Intelligence*, (2020).
- XU, S.; BLACKMORE, K.; AND JONES, H., 2007. An analysis framework for mobility metrics in mobile ad hoc networks. *EURASIP Journal on Wireless Communications and Networking*, 2007 (2007), 16.
- YU, T.; KUANG, Q.; ZHENG, J.; AND HU, J., 2021. Deep precipitation downscaling. *IEEE Geoscience and Remote Sensing Letters*, (2021).
- ZHANG, Y.; LI, K.; LI, K.; WANG, L.; ZHONG, B.; AND FU, Y., 2018. Image super-resolution using very deep residual channel attention networks. In *Proceedings of the European Conference on Computer Vision (ECCV)*, 286–301.
- ZHANG, Y.; LI, K.; LI, K.; ZHONG, B.; AND FU, Y., 2019. Residual non-local attention networks for image restoration. *arXiv preprint arXiv:1903.10082*, (2019).